Inorganic Chemistry
Cite This: Inorg. Chem. 2019, 58, 9135−9149
Article
pubs.acs.org/IC

Ruthenium−Cyclopentadienyl Bipyridine−Biotin Based Compounds: Synthesis and Biological Effect

Leonor Côrte-Real,[†] Brittany Karas,[‡,§] Ana Rita Brás,[†,∥] Adhan Pilon,[†] Fernando Avecilla,[⊥] Fernanda Marques,[#] Ana Preto,[∥] Brian T. Buckley,[‡] Keith R. Cooper,[§] Cathleen Doherty,[‡] M. Helena Garcia,*[,†] and Andreia Valente*[,†]

[†]Centro de Química Estrutural, Faculdade de Ciências da Universidade de Lisboa, Campo Grande, 1749-016 Lisboa, Portugal

[‡]Environmental and Occupational Health Sciences Institute, Rutgers University, 170 Frelinghuysen Road, Piscataway New Jersey 08854, United States

[§]Department of Biochemistry and Microbiology, Rutgers University, 76 Lipman Drive, New Brunswick New Jersey 08854, United States

[∥]Centre of Molecular and Environmental Biology (CBMA), Department of Biology, University of Minho, Portugal. Campus de Gualtar, Braga 4710-057, Portugal

[⊥]Grupo Xenomar, Centro de Investigacións Científicas Avanzadas (CICA), Departamento de Química, Facultade de Ciencias, Universidade da Coruña, Campus de A Coruña, 15071 A Coruña, Spain

[#]Centro de Ciências e Tecnologias Nucleares, Instituto Superior Te′cnico (C2TN/IST), Universidade de Lisboa, Estrada Nacional 10 (km 139.7), 2695-066 Bobadela LRS, Portugal

Supporting Information

ABSTRACT: Prospective anticancer metallodrugs should consider target-specific components in their design in order to overcome the limitations of the current chemotherapeutics. The inclusion of vitamins, which receptors are overexpressed in many cancer cell lines, has proven to be a valid strategy. Therefore, in this paper we report the synthesis and characterization of a set of new compounds $[Ru(\eta^5\text{-}C_5H_5)(P(C_6H_4R)_3)(4,4'\text{-}R'\text{-}2,2'\text{-bpy})]^+$ (R = F and R′ = H, **3**; R = F and R′ = biotin, **4**; R = OCH_3 and R′ = H, **5**; R = OCH_3 and R′ = biotin, **6**), inspired by the exceptional good results recently obtained for the analogue bearing a triphenylphosphane ligand. The precursors for these syntheses were also described following modified literature procedures, $[Ru(\eta^5\text{-}C_5H_5)(P(C_6H_4R)_3)_2Cl]$, where R is −F (**1**) or $-OCH_3$ (**2**). The structure of all compounds is fully supported by spectroscopic and analytical techniques and by X-ray diffraction studies for compounds **2**, **3**, and **5**. All cationic compounds are cytotoxic in the two breast cancer cell lines tested, MCF7 and MDA-MB-231, and much better than cisplatin under the same experimental conditions. The cytotoxicity of the biotinylated compounds seems to be related with the Ru uptake by the cells expressing biotin receptors, indicating a potential mediated uptake. Indeed, a biotin−avidin study confirmed that the attachment of biotin to the organometallic fragment still allows biotin recognition by the protein. Therefore, the biotinylated compounds might be potent anticancer drugs as they show cytotoxic effect in breast cancer cells at low dose dependent on the compounds' uptake, induce cell death by apoptosis and inhibit the colony formation of cancer cells causing also less severe side effects in zebrafish.

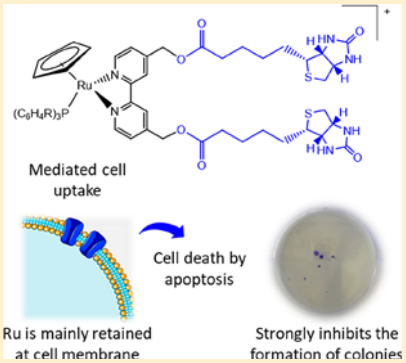

INTRODUCTION

One of the main obstacles in the development of new anticancer drugs is the lack of selectivity toward cancer cells that leads to undesirable side effects. Therefore, the design of target-specific drug delivery systems is still a very relevant challenge. An approach to this subject has been the use of vitamin−drug conjugates as a vehicle for a vitamin-mediated drug targeting due to the overexpression of vitamin receptors in the surface of cancer cells. In this frame, folic acid (vitamin B9), cobalamin (vitamin B12), riboflavin (vitamin B2), and biotin (vitamin B7) have been tested.[1−6] In particular, biotin has attracted more attention in the last years due to its higher tumor specificity imparted by its receptor-mediated uptake.[7] The main biotin transporter is the sodium-dependent multivitamin transporter (SMVT) that is overexpressed in several cancer cell lines such as breast MCF7 and MDA-MB-231,[5] thus supporting the relevance on the use of biotin as a targeting agent.

Several known anticancer agents in clinical use, such as paclitaxel,[8] doxorubicin,[9] and gemcitabine,[10] have been

Received: March 13, 2019
Published: June 26, 2019

DOI: 10.1021/acs.inorgchem.9b00735
Inorg. Chem. 2019, 58, 9135−9149

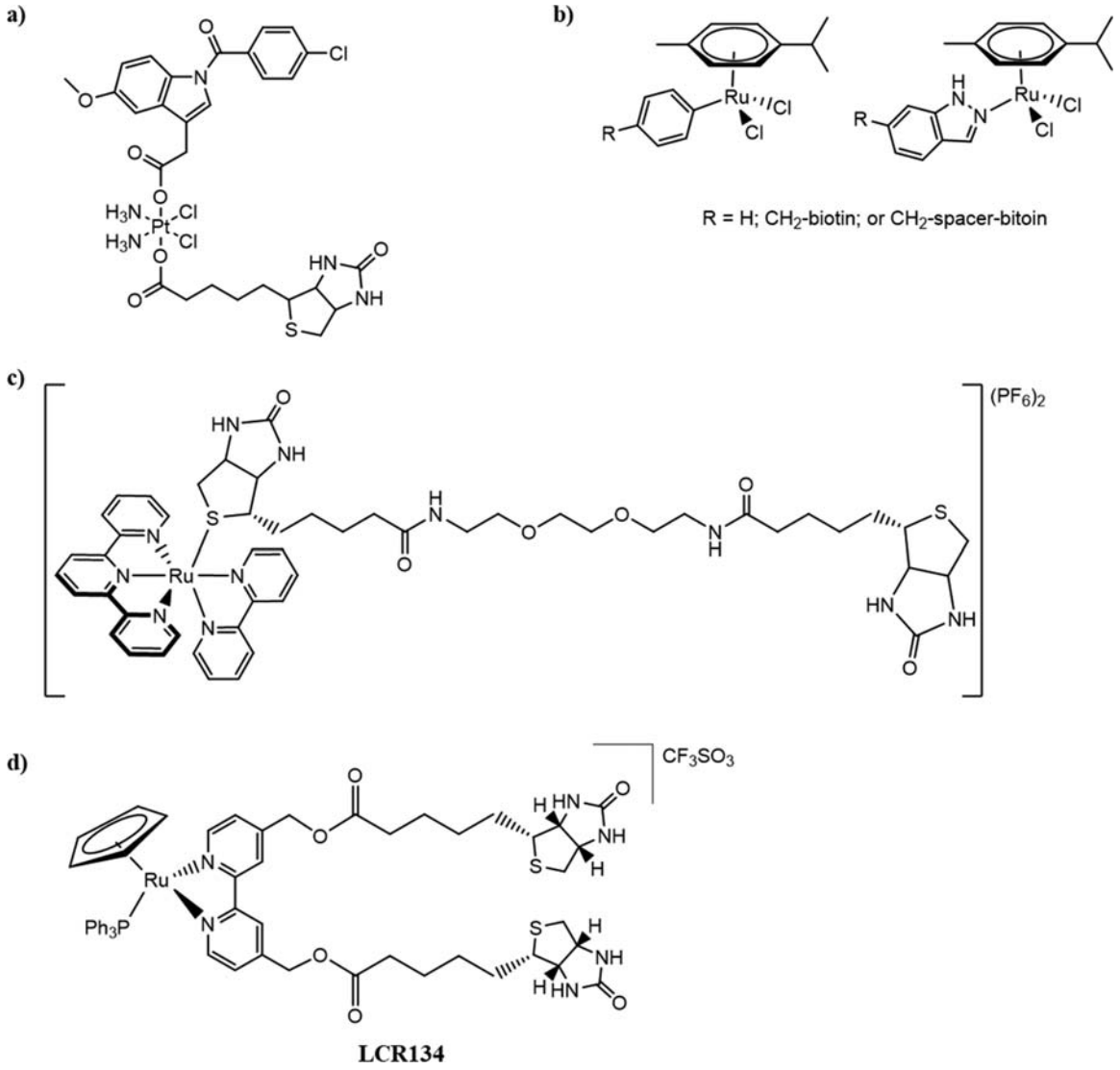

Figure 1. Prospective metallodrug–biotin conjugates.

functionalized with biotin to improve their efficiency and efficacy while reducing their toxicity.[6]

Furthermore, a prospective Pt(IV) prodrug (Figure 1a) based on cisplatin scaffold and bearing biotin and the nonsteroidal anti-inflammatory drug indomethacin (biotin-Pt(IV)-indomethacin conjugate) showed selectivity toward cancer cells vs. normal cells, while being cytotoxic and effective against cisplatin-resistant cancer cells.[11] The inclusion of biotin lead to a substantial increase in Pt uptake by the cells relative to cisplatin demonstrating a possible promotion of the compound's uptake via biotin receptor-mediated pathway. However, there is not a direct correlation with cytotoxicity.

Nowadays, ruthenium compounds are established alternatives to platinum-based drugs, trying to overcome their limitations in terms of toxicity and low efficacy for certain types of cancers. In this frame, some prospective ruthenium(III) compounds have reached clinical trials.[12−14]

The search for ruthenium(II) organometallic compounds is also an attractive option for medicinal chemistry due to the structural variety, chemical stability, diverse ligand bonding modes and redox properties achievable. Much of the literature is dedicated to the piano stool ruthenium(II)−(η^6-C_6H_6) derivatives developed by Dyson,[15] Sadler,[16] and co-workers. These compounds have shown good cytotoxicity *in vitro* and ability to reduce primary tumors *in vivo*, presenting in some cases antimetastatic activity as well. Also, the family of piano stool ruthenium(II)−(η^5-C_5H_5) derivatives has been attracting attention by some research groups due to their important cytotoxicity both *in vitro*[17,18] and *in vivo*.[19,20]

Targeting approaches using biotin have been also reported as, for example, the work by Hartinger and co-workers, where half-sandwich ruthenium(II) biotin conjugates (Figure 1b) were tested against colon cancer cell lines with higher levels of SMVT (SW620 cells presents ∼3 times more SMVT than HCT166 and COLO-205 cells).[21] However, no direct correlation between the biotin conjugation and the cellular Ru content and cytotoxicity was observed, implying that alternative pathways for cellular uptake of this compound might be operating.[21] Bonnet and co-workers also recently reported on a family of $[Ru(tpy)(bpy)(SRR')](PF_6)_2$ complexes, where, for the most promising approach, SRR' is a symmetrical ligand containing two identical biotin moieties linked via a triethylene glycol spacer (Figure 1c).[22] The authors proved that the compound binding to streptavidin is about the same as the natural biotin. The photochemical release of the SSR' ligand from the complex occurs upon blue

DOI: 10.1021/acs.inorgchem.9b00735
Inorg. Chem. 2019, 58, 9135−9149

Scheme 1. Synthetic Route of the New Ru(II) Complexes[a]

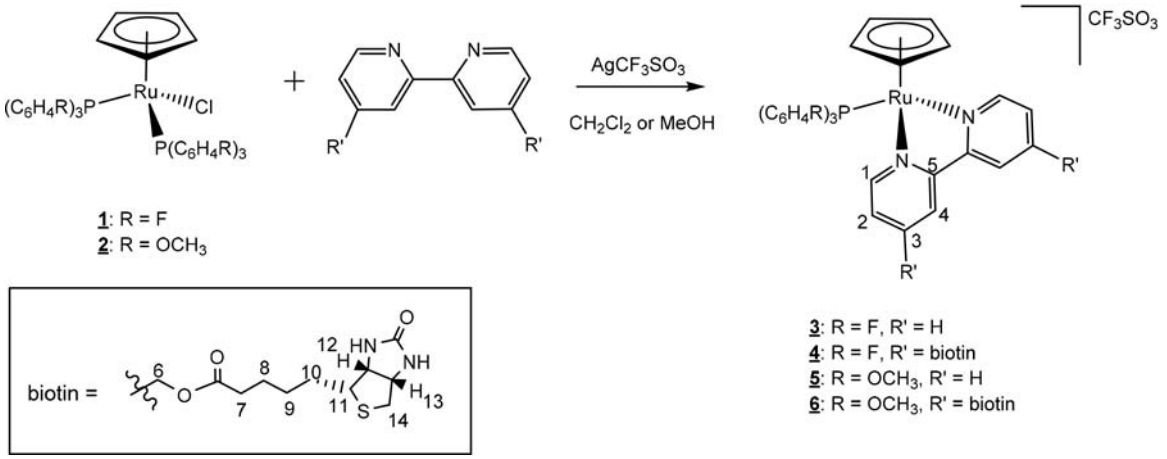

[a]Compounds are numbered for NMR assignments.

light irradiation, independent of the binding to streptavidin, thus envisaging their use as photoactivated chemotherapeutic complexes in streptavidin-mediated targeted therapy.

We have been interested in exploring the potential of ruthenium(II)−(η^5-C_5H_5) derivatives.[20,23−27] During our structure−activity studies we have noticed that the compounds belonging the family with the general formula [Ru(η^5-C_5H_5)(2,2′-bipyridine)(phosphane)]$^+$ were those with the best cytotoxicities against several human cancer cell lines and also the most stable under physiological conditions.[17,23] Recently, we described the conjugation of biotin to a ruthenium(II)-cyclopentadienyl compound of this family (Figure 1d).[28] This complex was cytotoxic against MCF7 and MDA-MB-231 breast cancer cell lines and showed exceptional selectivity as P-gp inhibitor and good tolerability for zebrafish (up to 1.17 mg/L at 5 days post fertilization). In the present study we synthesized a family of related compounds bearing different functional groups at the phosphane ligand to investigate their influence on cytotoxicity, cellular uptake via receptor mediated internalization and *in vivo* toxicity in zebrafish.

RESULTS AND DISCUSSION

On the basis of the successful results in biological activity we recently obtained[28] for a biotinylated ruthenium−cyclopentadienyl complex (**LCR134**, Figure 1), an enlarged family of compounds was explored. Here, the chemical and biological responses to the substitution on the triphenylphosphane coligand were studied (Scheme 1). The starting materials with the general formula [Ru(η^5-C_5H_5)(P(C_6H_4R)$_3$)$_2$Cl], where R is −F (**1**) or −OCH_3 (**2**), were synthesized following a modified literature procedure[29,30] giving orange crystalline powders in 67% and 51% yield, respectively. As for the cationic complexes [Ru(η^5-C_5H_5)(P(C_6H_4R)$_3$)(4,4′-R′-2,2′-bpy)]$^+$, where R′ is −H (**3** and **5**) or biotin (**4** and **6**), the syntheses were performed in reflux in dichloromethane (complexes **3** and **5**) or methanol (complexes **4** and **6**) for 4−7 h, by σ coordination of the bipyridine chelating ligand using silver triflate as chloride abstractor (Scheme 1). The orange complexes were obtained in moderate to good yields (52−87%).

The formulation and purity of all the new compounds is supported by FT-IR, UV−vis, and ^{1}H, ^{13}C, and ^{31}P NMR spectroscopic data and elemental analyses.

The solid-state FT-IR spectra (KBr pellets) of the six new organometallic ruthenium−cyclopentadienyl complexes show the presence of the typical bands attributed to υ_{CH} stretching of the phosphane, cyclopentadienyl, and bipyridyl ligands (when present) in the range 3100−3000 cm^{-1} and the bands for $\upsilon_{C=C}$ at 1600−1475 cm^{-1}. The presence of the triflate counterion for the cationic complexes **3**−**6** was confirmed by the typical signal for this group (∼1240 cm^{-1}). For the compounds bearing the bipy−biotin ligand the typical bands attributed to υ_{N-H} and υ_{C-N} stretching of the amines (3500−3300 cm^{-1} and 1200−1025 cm^{-1}, respectively), as well as the $\upsilon_{C=O}$ stretching of the ester and ketone (1732 and ∼1700, respectively), were also present. The υ_{C-H} stretching bands, attributed to the alkyl chain of the bipy−biotin ligand, were also observable at 2930−2860 cm^{-1}.

Analysis of the overall ^{1}H NMR data show that the resonances of the η^5-cyclopentadienyl ring are in the characteristic range for neutral and monocationic ruthenium(II) complexes (at 4.09−4.22 and 4.89−4.97 ppm, respectively). The successful coordination of the bipyridyl derivatives is supported by the deshielding of the H1 protons (∼0.85 ppm) and a shielding of the H4 protons (0.25−0.32 ppm). Additionally, the resonances of the phosphane coligands appear between 6.66 and 7.49 ppm, being more shielded for the compounds bearing the -OCH_3 due to its electron donating character. The ^{31}P NMR spectra showed a unique sharp singlet for all the compounds, with the expected deshielding behavior upon coordination. The most shielded ^{31}P NMR signal is observed for compounds **5** and **6** containing 4-(methoxyphenyl)phosphane, due to the presence of the −OCH_3 group in the para position of the benzene ring, which agrees with the ^{1}H NMR data described above. The APT-^{13}C{^{1}H} and ^{13}C{^{1}H} NMR data are in accordance with the aforementioned effects in the ^{1}H NMR analysis.

The optical absorption spectra of complexes **1**−**6** and bipyridyl ligands were recorded in 10^{-4} to 10^{-6} M in dichloromethane and dimethyl sulfoxide solutions. In dichloromethane all the compounds present an intense band below 250 nm attributed to $\pi-\pi^*$ transitions occurring at the organometallic fragment {RuCp(P(C_6H_4R)$_3$)}$^+$. Relatively to the

DOI: 10.1021/acs.inorgchem.9b00735
Inorg. Chem. 2019, 58, 9135−9149

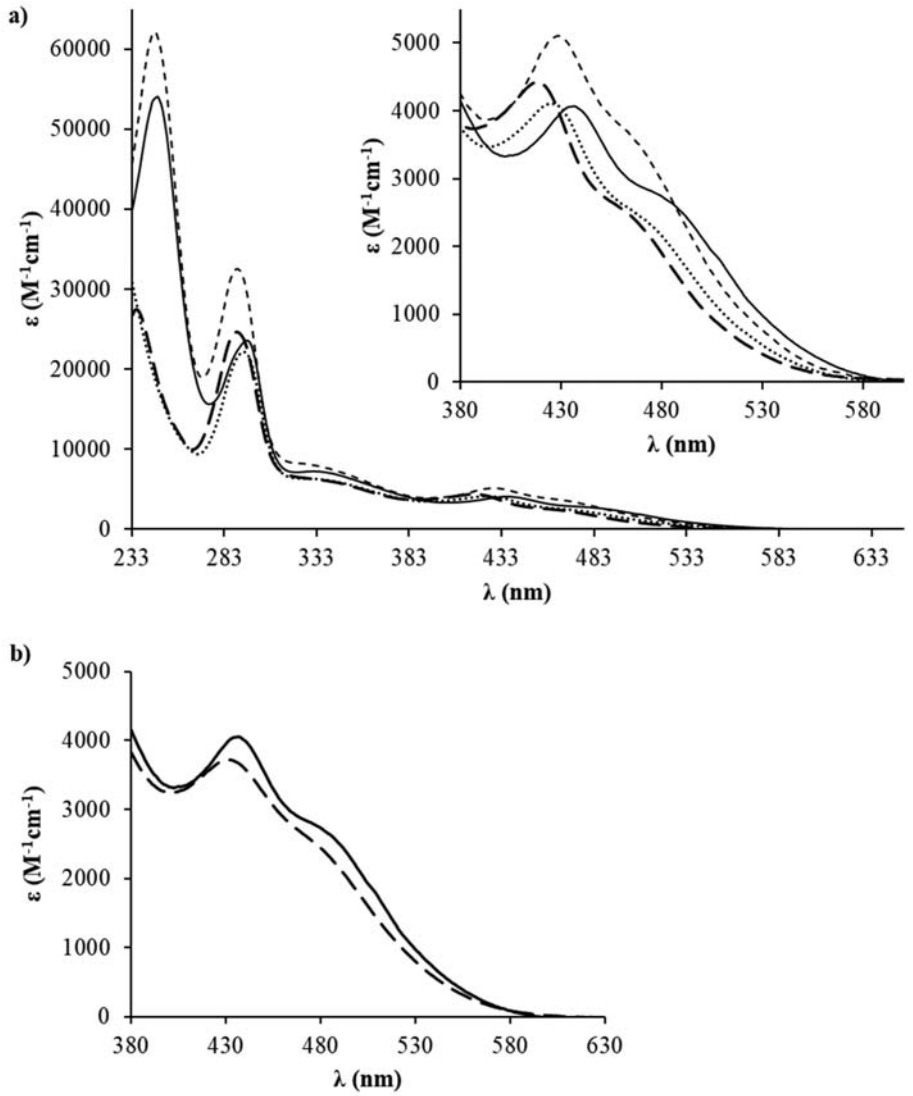

Figure 2. Electronic spectra of (a) **3** (— —), **4** (– –), **5** (---) and **6** (–) in dichloromethane solutions. Expansion of the spectra in the region of the CT transitions (b) **6** in DMSO (dashed line) and in dichloromethane (solid line) solutions, showing the hypsochromic shift.

compounds bearing the bipyridyl derivatives a second strong absorption band, appearing at ∼290 nm, is attributed to the $\pi \rightarrow \pi^*$ transitions that take place in the coordinated bipyridyl derivatives (Figure 2a). In addition to these bands, two maximum absorptions, at ∼420 and ∼480 nm were found for complexes **3** and **4**, and at ∼430 and 490 nm for complexes **5** and **6**, were attributed to metal-to-ligand charge transfer bands (MLCT), from Ru 4d orbitals to π^* orbitals of N-heteroaromatic rings and to phosphane, as previously reported for related compounds.[23,31,32]

Electronic spectra in DMSO were performed in order to infer about the charge transfer character of these bands. A hypsochromic shift of ca. 5 nm at the MLCT band can be observed, confirming the charge transfer nature of it, as exemplified in Figure 2b for compound **6**.

X-ray Crystal Structure Determination. Single crystal structures of mononuclear species of $[Ru(\eta^5\text{-}C_5H_5)(P(C_6H_4OCH_3)_3)_2Cl]$ (**2**), $[Ru(\eta^5\text{-}C_5H_5)(P(C_6H_4F)_3)(bipy)][CF_3SO_3]$ (**3**), and $[Ru(\eta^5\text{-}C_5H_5)(P(C_6H_4OCH_3)_3)(bipy)][CF_3SO_3]$ (**5**) are reported in this work. A dinuclear minor species obtained during the recrystallization processes of **LCR134** where the biotin ligand acts as bridge between two Ru ions was also obtained, $\{[Ru(\eta^5\text{-}C_5H_5)Cl]\text{-}\mu(N,N\text{-biotin-}S,S)\text{-}[Ru(\eta^5\text{-}C_5H_5)(P(C_6H_5)_3)]\}[Cl(CF_3SO_3)]$ (**LCR134′**).

Compounds **2**, **3**, and **5** crystallize from the solutions as red blocks. Figure 3a–c shows ORTEP representations of **2**, **3**, and **5**, respectively. In **LCR134′**, the asymmetric unit contains a dinuclear ruthenium cation complex, one $(CF_3SO_3)^-$ and one Cl^- anion, which is disordered and occupies two positions in the crystal packing. Figure 3d shows an ORTEP representation of the dinuclear complex.

In the four molecular structures, the ruthenium center adopts a "piano stool" distribution formed by the ruthenium–Cp unit bound to the different ligands.[33] The distances for Ru–P bonds are Ru(1)–P(1) = 2.3243(9) Å and Ru(1)–P(2) = 2.3208(9) Å in **2**, Ru(1)–P(1) = 2.3022(5) Å in **3** and 2.3220(5) Å in **5** and Ru(2)–P(1) = 2.3141(19) Å in **LCR134′** and the distances Ru–N bonds are Ru(1)–N(1) = 2.0719(14) Å in **3**, 2.0827(14) Å in **5** and 2.074(8) Å in **LCR134′** and Ru(1)–N(2) = 2.0910(15) Å in **3**, 2.0920(14) Å in **5** and 2.055(7) Å in **LCR134′**. The distance between Ru and the centroids of the π-bonded cyclopentadienyl moiety are

DOI: 10.1021/acs.inorgchem.9b00735
Inorg. Chem. 2019, 58, 9135–9149

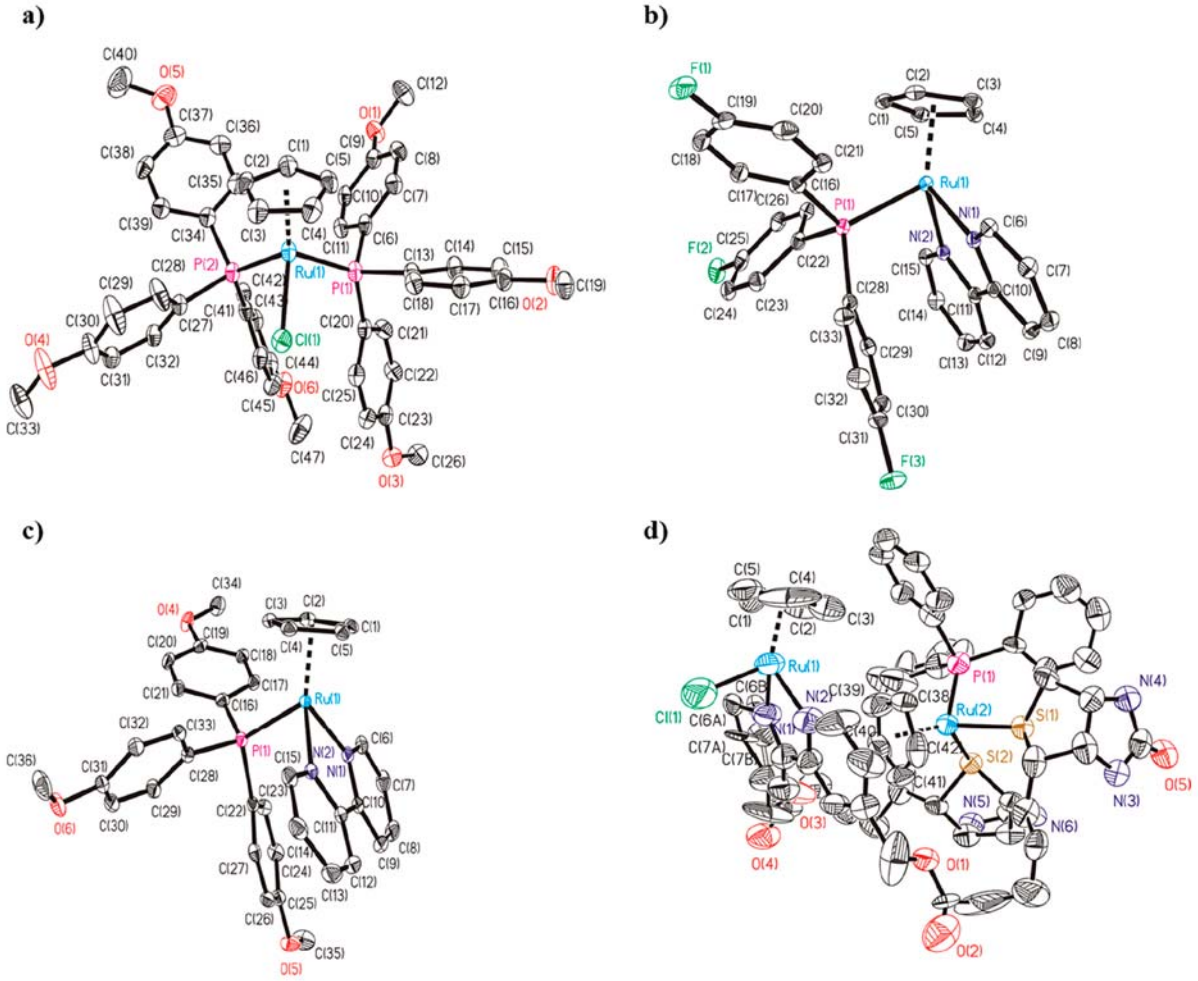

Figure 3. ORTEP for compounds (a) **2**, (b) **3**, (c) **5**, and (d) **LCR134′**. All the non-hydrogen atoms are presented by their 50% probability ellipsoids. Hydrogen atoms are omitted by clarity.

1.8516(2) Å in **2**, 1.8318(1) Å in **3**, 1.8383(1) Å in **5** to Ru center, and 1.837(5) Å to Ru(1) and 1.852(4) to Ru(2) in **LCR134′**, (ring slippage 0.033 Å in **2**, 0.029 Å in **3** and 0.046 Å in **5**, 0.061 and 0.065 Å in **LCR134′**). The mean value of the Ru−C bond distance is 2.2096(30) Å for **2**, 2.1960(17) Å for **3**, 2.2015(17) Å for **5** and 2.181(9) and 2.207(8) Å for **LCR134′**. Table S1 in Supporting Information contains selected bond lengths and angles for the four compounds.

X-ray structure analysis of the structures show two enantiomers of the complex $[Ru(\eta^5\text{-}C_5H_5)(P(C_6H_4OCH_3)_3)_2Cl]$ and in the cation complexes $[Ru(\eta^5\text{-}C_5H_5)(P(C_6H_4F)_3)(bipy)]^+$ and $[Ru(\eta^5\text{-}C_5H_5)(P(C_6H_4OCH_3)_3)(bipy)]^+$, which are present in the racemic crystals. The chirality is the result of a twist of the PPh_3 and Cp. The complexes show a mirror plane containing P, Ru and the centroid of Cp rings (see Figure S1).[23,34] **LCR134′** crystallizes in a chiral space group C2 and only contains one species. The Flack parameter of 0.04(5) confirms this fact.[35]

Stability Studies in Aqueous Media. Studies in aqueous relevant media of the new bipyridine-based compounds were performed prior to *in vitro* evaluation in order to access their stability. Thereby, complexes **3**−**6** were tested in culture cellular media over 24 h using 5% DMSO as cosolvent, by UV−vis spectroscopy (Figure S2). DMSO is used in the biological assays to allow complete solubilization of the compounds. All the complexes showed adequate stability over time, allowing their further biological study.

Biological Evaluation of the Compounds. *Analysis of the Cytotoxicity in Breast Cancer Cell Lines.* The cytotoxic activity of compounds **3**−**6** and the phosphane and bipyridine-based ligands was assessed in two human breast cancer cell lines, MCF7 and MDA-MB-231, at 24 h, using the colorimetric MTT assay. These cell lines were selected considering their different responses to cisplatin (CDDP) and their different genetic profiles. While MCF7 cell line has functional estrogen (ER α+) and EGF receptors and is noninvasive, MDA-MB-231 cells are hormone-independent, showing the triple negative phenotype (ER-, PR-, HER2-) being more invasive. Cells were treated with the compounds within the concentration range of 0.01−100 μM (or 10−200 μM for the ligands), and to CDDP within the concentration range 10−150 μM, for a period of 24 h (Table 1). The IC_{50} values of $[Ru(\eta^5\text{-}C_5H_5)(PPh_3)(2,2'\text{-bipyridine})][CF_3SO_3]$ (**TM34**), $[Ru(\eta^5\text{-}C_5H_5)(PPh_3)(2,2'\text{-bipy-4,4'-dibiotin ester})][CF_3SO_3]$ (**LCR134**), and CDDP were also included for comparison (Table 1). We could observe that the organometallic compounds showed low IC_{50} levels in the two cell lines tested, being much more cytotoxic than the organic ligands *per se*, showing that the cytotoxicity of the complexes results from a synergy between all coligands and the metal center. The complexes bearing the 2,2′-bipyridine

DOI: 10.1021/acs.inorgchem.9b00735
Inorg. Chem. 2019, 58, 9135−9149

Table 1. IC_{50} Values (μM) for Complexes 3−6, TM34, LCR134, CDDP, and Phosphane and Bipyridine-Based Ligands at 24 h Incubation, in MCF7 and MDA-MB-231 Breast Cancer Cells (n.d.: Not Determined)

compound	MCF7 (μM)	MDA-MB-231 (μM)
TM34	0.9 ± 0.3[46]	1.5 ± 0.3[47]
3	0.9 ± 0.3	2.1 ± 0.6
5	1.7 ± 0.5	1.4 ± 0.4
LCR134	22.5 ± 1.8	10.6 ± 0.3
4	22.4 ± 1.6	14.2 ± 0.7
6	18.7 ± 1.6	7.7 ± 0.3
CDDP	37.9 ± 1.4[28]	122.3 ± 24.9[28]
triphenylphosphane	143.5 ± 31.6	176.0 ± 35.5
tris(4-fluorophenyl)phosphane	101.0 ± 22.0	185.9 ± 14.7
tris(4-methoxyphenyl)phosphane	198.1 ± 67.3	161.9 ± 25.8
2,2′-bipyridine	n.d.	125.1 ± 21.3
2,2′-bipy-4,4′-dibiotin ester	n.d.	>200

ligand (**3** and **5**) are the most cytotoxic, similar to **TM34** for both cell lines. Compounds **4** and **6**, bearing the bipy−biotin ligand, are also cytotoxic for both cell lines and of the same order of magnitude as **LCR134**. All compounds exhibit lower IC_{50} values than CDDP by ∼2−42 fold for MCF7 and ∼9−87 fold for MDA-MB-231 cell line, and are generally better or in the same order of magnitude of other Ru(II)−η^6-arene derivatives.[36−44] Thus, the results suggest that these compounds might be potent anticancer drugs as the dose that show cytotoxic effect is low. Interestingly, the compounds bearing the bipy−biotin based ligand are more cytotoxic for the most invasive MDA-MB-231 cell line, which may be related to their cellular uptake and the different genetic background of these cells, and these differences may affect the sensitivity of the cells to the compounds. In fact, a recent paper by Sava and coworkers discloses that, for RAPTA-T ($[Ru(\eta^6\text{-}C_6H_5Me)(pta)Cl_2]$, pta = 1,3,5-triaza-7-phosphaadamantane), the differences in activity obtained between MCF7 cell line and the invasive MDA-MB-231 might be related to the antimetastatic properties observed for this compound for which the MDA-MB-231 cell line is a good model.[45]

Biotin−Avidin Interaction Assay. The relative affinity of compounds **3−6** and **LCR134** to avidin was determined by using a Biotin Quantitation Kit. The compounds and biotin (used as positive control) were added to a solution containing a mixture of HABA (4′-hydroxyazobenzene-2-carboxylic acid) and avidin. Because of its higher affinity for avidin, biotin (or biotinylated compounds) displaces HABA and the absorbance at 500 nm decreases proportionately. As expected, the affinity for avidin was higher for the natural ligand biotin. Regarding the ruthenium compounds, all the biotinylated compounds (**LCR134**, **4**, and **6**) showed an affinity for avidin that was approximately half of the one showed by biotin, while the nonbiotinylated compounds (**3** and **5**) did not interact. The values do not differ significantly among the biotinylated compounds tested, suggesting that the presence of the different phosphane coligands do not interfere with biotin recognition. The recognition of biotin-based complexes by avidin indicates that this synthesis approach used to target the biotin transporter (SMVT) is valid, as already observed for other ruthenium organometallic compounds.[21]

In Vivo Toxicity Assessment Using Zebrafish Embryos. The zebrafish (*Danio rerio*) model has been considered an attractive and viable alternative model to study human diseases, complementary to rodent models, due to zebrafish ease of husbandry and more affordable maintenance. Zebrafish develop very rapidly and have high fecundity and fertilization rates (up to 200 fertilized eggs per mating pair) compared to mammalian models (5−10 offspring per mating pair), reducing the time needed to complete a study. Furthermore, the zebrafish genome shows approximately 70% of homology with the human genome and 82% of orthologous (derived from a common ancestral sequence) human disease-related genes.[48,49] Thus, the zebrafish embryo larval assay (ZELA) was used for evaluating adverse effects of chemical exposure of complexes **3−6** at the organ system level and for that, a modified OECD.2013 protocol was used.[50] At 3 h post fertilization (hpf), eggs were exposed to increasing concentrations of these complexes. The fertilization rate was >80% and the control survival rate was consistently ≥90%. The compound concentrations were analytically evaluated by ICPMS at the end of the experiment, and they are shown in the Experimental Section. Daily observations of the embryos were recorded and lethality/survival, as well as lesions, were evaluated.

From the dose response curves, four acute toxicity end points were obtained: LC_{50}, lethality for 50% of the embryos/larvae; NOEC, no observed effect concentration; LOEC, lowest observed effect concentration; and NOEL, no observed effect level (Table 2).

Graphical representations of the lethality-response curves for each complex can be seen in Figure 4 and allowed for the estimation of the LC_{50} values at the end of 120 hpf experiment. At first glance, it appeared that **3** is the least toxic of this series of compounds, having the highest LC_{50} value. Its major toxic lesion however is necrosis, as can be seen in Table S2 (moderate to severe effect), causing severe damage (cellular lysis) to the embryos and eventually their death. This process, contrarily to apoptosis, is caused by external factors and results in premature death of cells in living tissues and was only found for complexes **3** and **5**, which have the 2,2′-bipyridine ligand. Complexes **4** and **6**, bearing the 2,2′-bipy-4,4′-dibiotin ester ligand, had essentially yolk sac edema and pericardial sac edema (moderate to severe); for complex **4**, hemorrhage of the syncytial layer was also observed. The yolk syncytial layer is a

Table 2. Estimates Obtained from in Vivo Toxicity Analyses at the End of the 120 hpf Experiment

	LC_{50} (95% CL[a]) (mg/L)	NOEC (mg/L)	LOEC (mg/L)	NOEL (mg/L)	NOEL (ng/larvae)
3	3.28 (2.50−3.72)	–	2.02	0.69	1.56
4	2.35 (2.09−2.48)	–	1.31	–	–
5	0.80 (0.35−1.16)	0.17	0.57	0.17	0.92
6	1.83 (1.28−2.17)	–	1.52	0.80	1.17
LCR134[28]	5.73 (4.74−6.26)	2.18	3.48	1.17	2.34

[a]CL = confidence limits; NOEC = no observed effect concentration; LOEC = lowest observed effect concentration; NOEL = no observed effect level.

DOI: 10.1021/acs.inorgchem.9b00735
Inorg. Chem. 2019, 58, 9135−9149

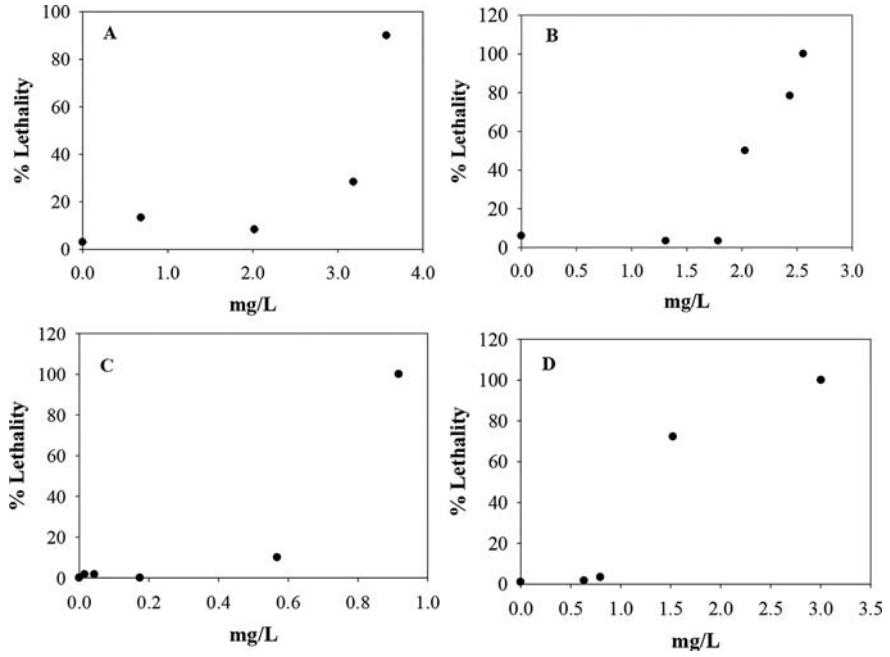

Figure 4. Lethality-response curves for tested ruthenium complex solutions in mg/L (A, complex **3**; B, complex **4**; C, complex **5**; and D, complex **6**).

highly dynamic syncytial tissue with essential and diverse functions during early zebrafish development. Damage in this cellular structure may indicate that the embryonic development is compromised. The most frequently observed grossly visible effects are summarized in Figure 5 and Tables S2–S5.

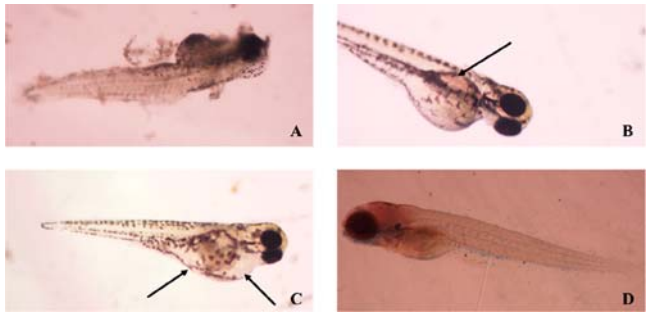

Figure 5. Representative pictures of zebrafish lesions found after treatment with complexes **3**–**6**. Key: (A) necrosis; (B) hemorrhage in syncytial layer; (C) yolk sac edema and pericardial sac edema; (D) control (stained). The zebrafish embryos representative pictures were obtained with Olympus SZ-PT dissecting microscope equipped with Scion digital camera model CFW-1310C and analyzed with Photoshop software. Magnification 4×.

At the end of the experiment (120 hpf), the larvae were sacrificed, digested, and analyzed by ICPMS to quantify the Ru (Figure S3). Complex **3** had the highest internalization rate in the larvae (4.93 ng/larvae), followed by complex **4** and **5**, with 3.79 and 3.57 ng/larvae, respectively, that are in the same range of magnitude of **LCR134**. Complex **6** had the lowest internalization rate (1.17 ng/larvae).

Intraocular distance, total body length, pericardial sac, and yolk sac area end points were analyzed to better describe the adverse morphometric effects (Figures S4–S7). All complexes showed reduced body length for either all concentrations (**4** and **6**) or for the two highest concentrations (**3** and **5**), which may be an indication of an inhibition of the overall growth of the organism.

Intraocular distance was used to indicate changes in craniofacial development following embryonic chemical exposure. A significant decrease of intraocular distance was found for **4** (all concentrations), **5** (0.17; 0.57 mg/L), and **6** (1.52 mg/L).

The yolk sac comprises vitellogenin derived yolk-proteins that entirely support nutritional needs of the embryo/larvae prior to beginning feeding after 120 hpf. Thus, its size is a significant end point in assessing whether the compound affected the magnitude of the available nutrients and their use in embryonic zebrafish. It was observed that the yolk sac size has only increased with exposure to complexes **3** and **4**, which may indicate either fluid accumulation outside the vasculature (yolk sac edema) and/or an uptake of lipoproteins.

Finally, the pericardial sac size was also measured, revealing that there was only a statistically significant increase of the pericardial sac size for one of the concentrations of complex **4** (1.79 mg/L). In fact, this complex was the only one showing a mild to moderate level of pericardial sac edema for almost all concentrations, possibly indicating that it may have compromised the cardiovascular system of the embryos.

Since that compounds **3** and **5** showed severe toxic effects (necrosis/cell lysis) compared to the biotinylated complexes **4**, **6**, and **LCR134** (major lesions were yolk sac and pericardial sac edemas), one can consider that the targeting approach was successful leading to better *in vivo* tolerability. Thus, these three compounds bearing the 2,2′-bipy-4,4′-dibiotin ester ligand were selected for further studies aiming to understand their anticancer properties.

Intracellular Distribution of the Ruthenium Complexes. The intracellular distribution of the complexes **4**, **6** and **LCR134** was performed using MCF7 and MDA-MB-231 cells, both expressing biotin receptors,[5] following exposure to each complex for 24 h at a concentration equivalent to their IC_{50} values. Cytosol, membrane, nucleus, and cytoskeletal fractions were extracted using a commercial kit as described in the

DOI: 10.1021/acs.inorgchem.9b00735
Inorg. Chem. 2019, 58, 9135–9149

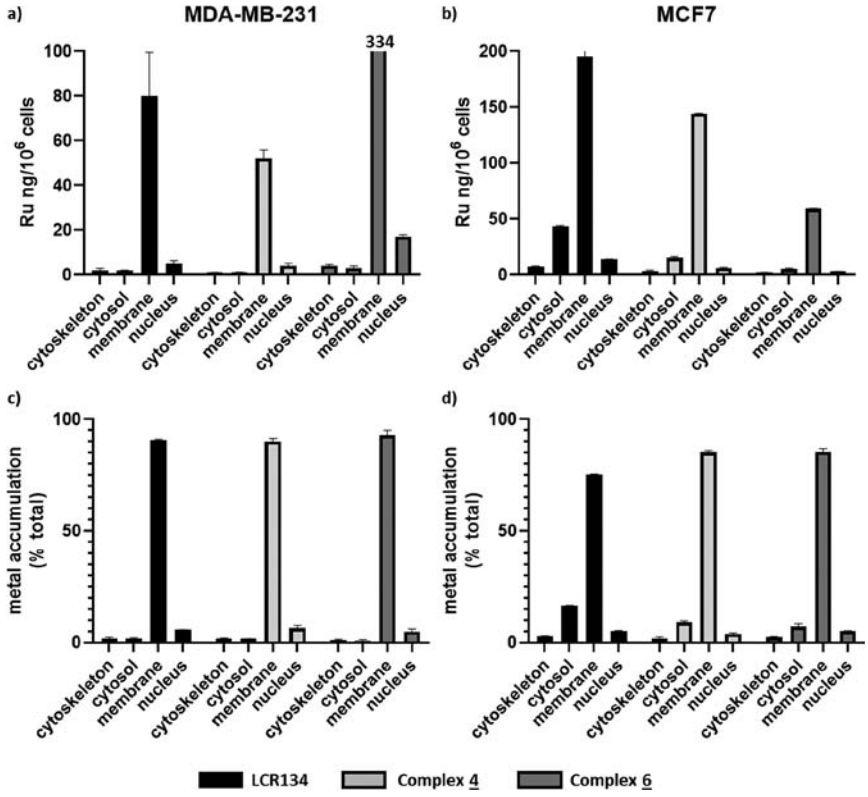

Figure 6. Cellular Ru distribution in the MCF7 and MDA-MB-231 cells treated with the compounds **LCR134**, **4**, and **6** at a concentration equivalent to the IC_{50} values found at 24 h challenge, 37 °C. Results are expressed in ng of Ru per million of cells (a and b) or in total percentage (c and d). Results are expressed as mean ± SD of two independent experiments.

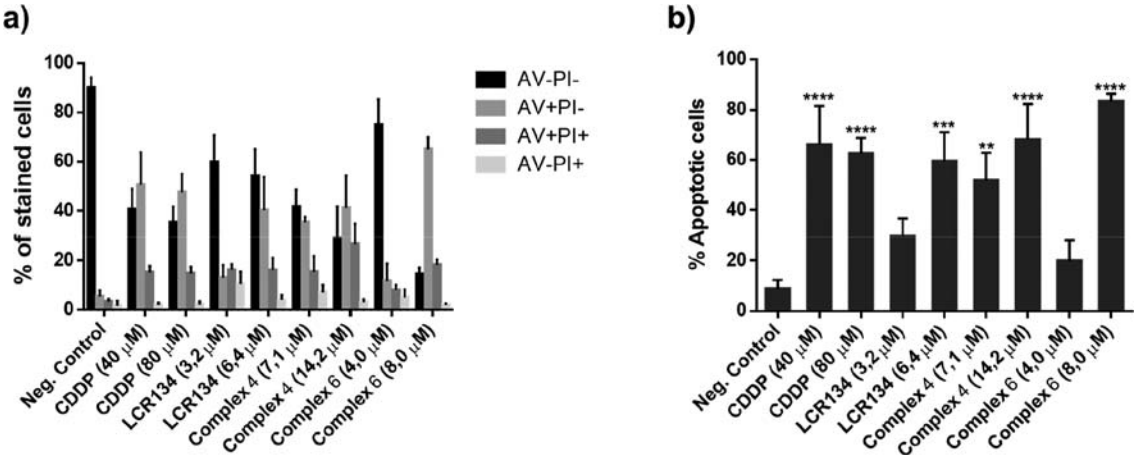

Figure 7. Ruthenium-based compounds potentiate apoptotic cell death in breast cancer cell line. Apoptotic cell death was analyzed by Annexin V fluorescein isothiocyanate (AV-FITC) and propidium iodide (PI) assay in MDA-MB-231 cells, after incubation with IC_{50} and 2 × IC_{50} concentrations for 48 h. Cisplatin was used as a positive control at a concentration of 40 μM and 80 μM. (a) Graphical representation of the Annexin V/PI dot plots of flow cytometry data of control, CDDP, **LCR134**, **4**, and **6** compounds were analyzed using Flowing software. Values are mean ± SD of three independent experiences. (b) Percentages of apoptotic cells (positive for AV). Values represent mean ± SD of at least three independent experiments. Statistical analysis was performed by one-way ANOVA with Dunnett's multiple comparisons test. Key: (**) $P \leq 0.01$; (***) $P \leq 0.001$; (****) $P \leq 0.0001$ compared with negative control.

Experimental Section. In general, all the compounds are mainly retained at the membrane of both cancer cell lines (Figure 6; >90% for MDA-MB-231 and >75% for MCF7). Similar trends were observed for related ruthenium cyclopentadienyl compounds previously reported.[47,51] For the MDA-MB-231 cell line, the cytotoxicity of the compounds correlates well with their internalization being higher for complex **6**, followed by **LCR134** and **4**. For the MCF7 cell line an increase in the Ru content on the cytosol fraction was observed (16% for **LCR134**, 9% for **4**, and 7% for **6**). These results might be related to the different genetic background of each cell line. For this cell line, the cytotoxicity does not correlate with the Ru uptake by the cells. Normalizing the results for the concentration administered in each condition (Figure S8), one can observe that the total ruthenium content is approximately the same in both cell lines for **LCR134** and complex **4**, while

DOI: 10.1021/acs.inorgchem.9b00735
Inorg. Chem. 2019, 58, 9135−9149

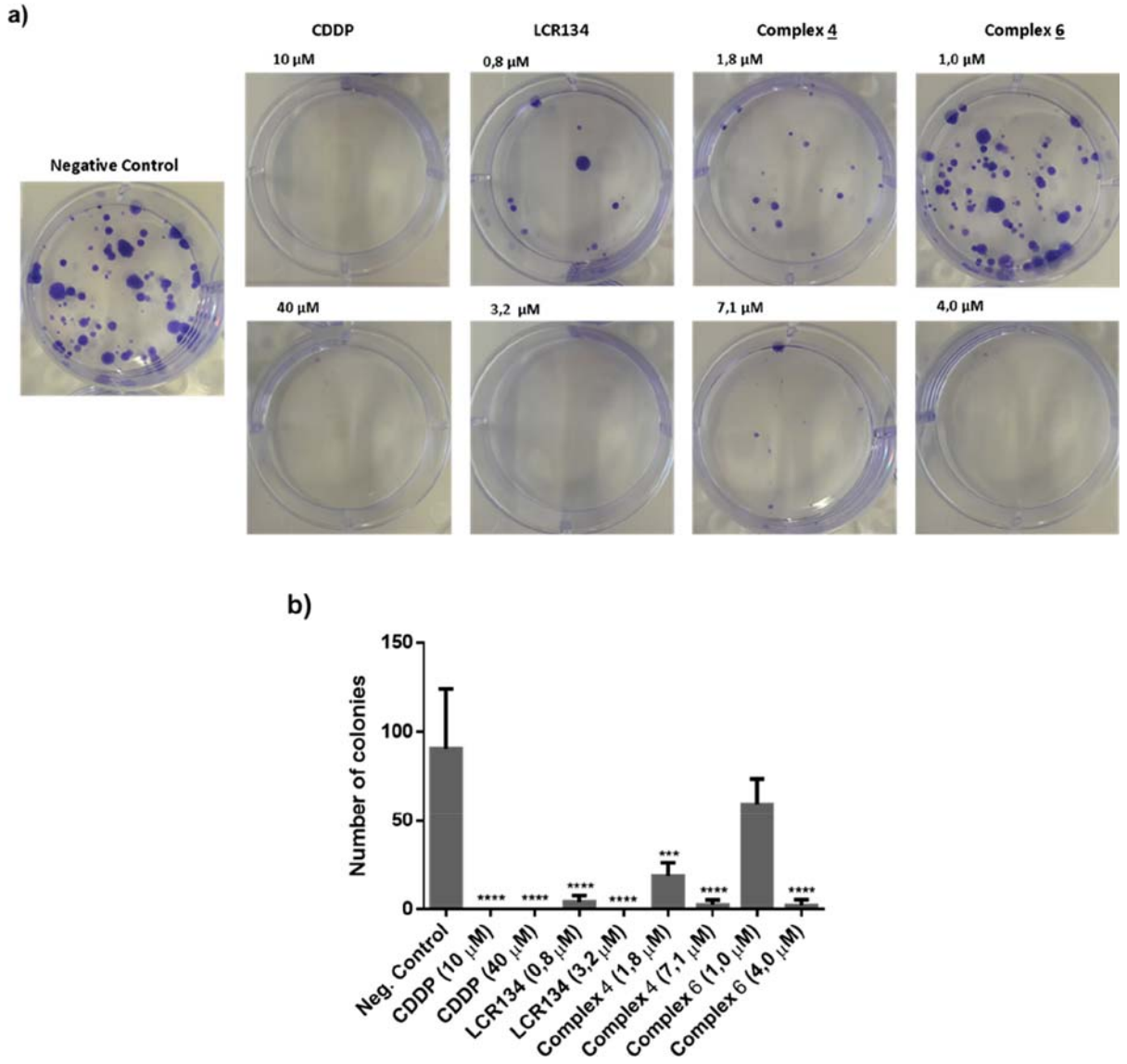

Figure 8. Colony formation ability of MDA-MB-231 after being exposed to our compounds. Analysis of the clonogenic ability, after 48 h incubation with 1/4 IC_{50} and IC_{50} values, in MDA-MB-231 cell line. CDDP was used as a positive control at 10 and 40 μM. (a) Representative images of colony formation assay in MDA-MB-231 cell line. (b) Values represent mean ± SD of at least three independent experiments. Statistical analysis was performed by one-way ANOVA with Dunnett's multiple comparisons test. Key: (***) $P \leq 0.001$; (****) $P \leq 0.0001$ compared with negative control.

for compound **6** the Ru content in the MDA-MB-231 cell line is approximately 9 times higher than in the MCF7 cell line, showing that the phosphane coligand also has a role on the cellular uptake of these compounds.

Evaluation of the Cell Death Mechanism Induced by Ruthenium-Based Compounds. Annexin V/Propidium iodide (AV/PI) cytometry-based assay was used to determine the cell death mechanism caused by the ruthenium compounds. MDA-MB-231 cells were incubated with the ruthenium compounds **LCR134**, **4**, and **6** for 48 h at their IC_{50} and 2 × IC_{50} values (Table S6). Cisplatin was used as positive control. The results showed that the compounds induce apoptosis instead of necrosis and that the majority of the cells appear at early apoptosis (Figure 7). Excluding the IC_{50} conditions of **LCR134** and of complex **6**, all the other conditions significantly induced apoptosis at higher levels.

The Effects of Biotin-Based Compounds in the Colony Formation Potential of Cancer Cells. To evaluate the colony formation potential of the most promising compounds **LCR134**, **4** and **6**, MDA-MB-231 breast cancer derived cell line were exposed to $^1/_4$ of the IC_{50} and IC_{50} values of the different compounds for 48 h, after which the medium was removed, and cells were maintained in culture for 11 days. MDA-MB-231 breast cancer derived cell line is commonly used as a model of Triple Negative Breast Cancer (TNBC). TNBC typically encompasses highly metastatic cancers with poorer prognosis to which no available effective therapy is available yet.[52] Our results showed that all the compounds reduce the ability of the cells to form colonies (Figure 8). All concentrations of compounds studied, except $^1/_4IC_{50}$ of complex **6**, have significantly prevented the formation of colonies, and under conditions treated with the IC_{50} values, the compounds inhibited the ability to form colonies in a high extent. Regarding to **LCR134** compound, the results were very promising, since at the $^1/_4$ IC_{50} and IC_{50} concentrations, the compound almost completely inhibited the formation of

DOI: 10.1021/acs.inorgchem.9b00735
Inorg. Chem. 2019, 58, 9135−9149

colonies, which was very similar to the results of cisplatin. This is a very good result since cisplatin is one of the most chemotherapeutic agents used in the treatment of this type of cancer, although it has severe side effects and acquisition of resistance.[53] Interestingly, the IC_{50} value of **LCR134** inhibited completely the formation of colonies but did not induce apoptosis in a significant manner, which could suggest that this compound has a mechanism of action with greater action in inhibiting proliferation rather than inducing cell death.

CONCLUSIONS

A family of new compounds with the general formula $[Ru(\eta^5\text{-}C_5H_5)(P(C_6H_4R)_3)(4,4'\text{-}R'\text{-}2,2'\text{-bpy})]^+$ (R = F and R′ = H, **3**; R = F and R′ = biotin, **4**; R = OCH_3 and R′ = H, **5**; R = OCH_3 and R′ = biotin, **6**, R = H, R′ = biotin, **LCR134**[28]) was synthesized. The precursors $[Ru(\eta^5\text{-}C_5H_5)(P(C_6H_4R)_3)_2Cl]$ (R = F, **1** or R = OCH_3, **2**) were also prepared following modified literature procedures. All the compounds were completely characterized by spectroscopic and analytical techniques and by X-ray diffraction studies for compounds **2**, **3**, and **5**. While all the cationic complexes showed cytotoxicities much better than cisplatin in the breast MCF7 and MDA-MB-231 cancer cell lines, none of the organic ligands was cytotoxic for the cell lines tested. Importantly, for the biotinylated compounds, there is a relation between Ru uptake by the cells and the cytotoxicity for the most aggressive and invasive MDA-MB-231 cell line. All biotinylated compounds were recognized by avidin, even if it was at lower extent than the natural avidin, showing that the recognition was not greatly affected upon complexation and indicating that biotin might act as a biological vector promoting the delivery of the compounds to the cells.

Overall, the biotinylated compounds can be considered promising anticancer drugs since they show low IC_{50} values, induce cell death by apoptosis and inhibit the colony formation of cancer cells being better tolerated in zebrafish than the nonbiotinylated compounds. The fact that the biotinylated compounds are (i) more active for the invasive MDA-MB-231 cell line than to the MCF7 cell line, (ii) mainly retained at the cell membrane of cancer cells (>90% for MDA-MB-231), and (iii) able to inhibit the formation of colonies (loss of adhesive interactions) might forecast an antimetastatic behavior as was reported for other ruthenium compounds.[45]

EXPERIMENTAL SECTION

General Procedures. All reactions and manipulations were performed under nitrogen atmosphere using *Schlenk* techniques. All solvents used were dried and freshly distilled under nitrogen prior to use, using standard methods. ^1H, ^{13}C, and ^{31}P NMR spectra were recorded on a Bruker Avance 400 spectrometer at probe temperature using commercially available deuterated solvents. ^1H and ^{13}C chemical shifts (s = singlet; d = doublet; t = triplet; m = multiplet, dd = doublet of doublets, dt = doublet of triplets) are reported in parts per million (ppm) downfield from internal standard Me_4Si, and the ^{31}P NMR spectra are reported in ppm downfield from external standard, 85% H_3PO_4. Coupling constants are reported in Hz. All assignments were attributed using APT-$^{13}C\{^1H\}$ or $^{13}C\{^1H\}$, COSY, HMBC and HMQC NMR techniques. Infrared spectra were recorded on KBr pellets using a Mattson Satellite FT-IR spectrophotometer and only relevant bands were cited in the text. Electronic spectra were obtained at room temperature on a Jasco V-560 spectrometer from solutions of 10^{-4}–10^{-6} M in quartz cuvettes (1 cm optical path). Elemental analyses were performed at Laboratório de Análises, at Instituto Superior Técnico, using a Fisons Instruments EA1 108 system. Data acquisition, integration, and handling were performed using a PC with the software package EAGER-200 (Carlo Erba Instruments).

The synthesis of the bipy–biotin ligand was previously described by us.[28]

Synthesis. *$[Ru(\eta^5\text{-}C_5H_5)(P(C_6H_4R)_3)_2Cl]$, R = F (1) or OCH_3 (2).* The synthesis of **1** has been previously described in the literature.[29] Here we report slight alterations and a complete characterization. The synthesis of **2** is new and was adapted from the literature.[30] To a stirred and degassed solution of hydrated ruthenium trichloride (0.33 g, 1.59 mmol; 2.32 g, 11.20 mmol for **1** and **2**, respectively) in ethanol (60 mL) was added tris(4-fluorophenyl)phosphine or tris(4-methoxyphenyl)phosphine (1.83 g, 5.80 mmol; 10.00 g, 28.00 mmol for **1** and **2**, respectively) and freshly distilled cyclopentadiene (4 mL; 20 mL, for **1** and **2**, respectively). The dark brown mixture obtained was refluxed with vigorously stirring for 7 or 4 h (for **1** or **2**, respectively) until no more precipitation of the orange complex was observed. After refluxing, the mixture was cooled to room temperature overnight. The precipitate was filtered, washed with water (2 × 20 mL), hexane, and light petroleum ether or diethyl ether (2 × 20 mL, for **1** and **2**, respectively). The crystalline orange powder obtained was dried under vacuum, originating compounds **1** and **2** in 67% and 51% yields, respectively. Single crystals were isolated by recrystallization from dichloromethane/*n*-hexane for compound **2**.

Complex 1. ^1H NMR [$(CD_3)_2CO$, Me_4Si, δ/ppm]: 7.49 (m, 12, $H_{meta}P(PhF)_3$); 7.01 (t, 12, $^3J_{HH}$ = 8.0, $H_{ortho}P(PhF)_3$); 4.22 (s, 5, $\eta^5\text{-}C_5H_5$). $^{13}C\{^1H\}$ NMR [$(CD_3)_2CO$, δ /ppm]: 164.1 (d, $^1J_{CF}$ = 248.5, Cq, $P(PhF)_3$); 136.9 (dt, $^3J_{CP}$ = 5.9; $^2J_{CF}$ = 7.9, $CH_{meta}P(PhF)_3$); 135.1 (dd, $^1J_{CP}$ = 41.8; $^4J_{CF}$ = 4.0, Cq, $P(PhF)_3$); 115.5 (dt, $^2J_{CP}$ = 21.0; $^3J_{CF}$ = 5.1, $CH_{ortho}P(PhF)_3$); 82.6 (t, $^2J_{CP}$ = 2.0, Cp). $^{31}P\{^1H\}$ NMR [$(CD_3)_2CO$, δ/ppm]: 38.17 (s, $P(PhF)_3$). UV–vis [CH_2Cl_2, λ_{max}/nm ($\varepsilon \times 10^3/M^{-1}cm^{-1}$)]: 234 (34.8); 291 (Sh); 369 (2.4); 454 (Sh). [DMSO, λ_{max}/nm ($\varepsilon \times 10^3/M^{-1}cm^{-1}$)]: 285 (Sh); 366 (2.1); 441 (Sh). FTIR [KBr, cm^{-1}]: 3070, 3036 (υ_{C-H} Cp and phenyl rings); 1587, 1494 ($\upsilon_{C=C}$ Cp and aromatic rings). Anal Calcd for $C_{41}H_{29}ClF_6P_2Ru$ (834.14): C, 59.0; H, 3.5. Found: C, 58.6; H, 3.5.

Complex 2. ^1H NMR [$CDCl_3$, Me_4Si, δ/ppm]: 7.30 (m, 12, $H_{ortho}P(PhOCH_3)_3$); 6.66 (d, 12, $^3J_{HH}$ = 12.0, $H_{meta}P(PhOCH_3)_3$); 4.09 (s, 5, $\eta^5\text{-}C_5H_5$); 3.77 (s, 18, OCH_3). $^{13}C\{^1H\}$ NMR [$CDCl_3$, δ /ppm]: 159.8 (Cq, $P(PhOCH_3)_3$); 135.3 (t, $^2J_{CP}$ = 5.5, $CH_{ortho}P(PhOCH_3)_3$); 130.4 (d, $^1J_{CP}$ = 44.3, Cq, $P(PhOCH_3)_3$); 112.9 (t, $^3J_{CP}$ = 5.0, $CH_{meta}P(PhOCH_3)_3$); 81.1 (m, Cp); 55.3 (OCH_3). $^{31}P\{^1H\}$ NMR [$CDCl_3$, δ/ppm]: 35.67 (s, $P(PhOCH_3)_3$). UV–vis [CH_2Cl_2, λ_{max}/nm ($\varepsilon \times 10^3/M^{-1}cm^{-1}$)]: 246 (68.6); 287 (Sh); 369 (2.8); 447 (Sh). [DMSO, λ_{max}/nm ($\varepsilon \times 10^3/M^{-1}cm^{-1}$)]: 380 (23.9); 446 (Sh). FTIR [KBr, cm^{-1}]: 3065 (υ_{C-H} Cp and aromatic rings); 1400–1600 ($\upsilon_{C=C}$ Cp and aromatic rings). Anal Calcd for $C_{47}H_{47}ClO_6P_2Ru$ (906.35): C, 62.2; H, 5.2. Found: C, 62.0; H, 5.2.

$[Ru(\eta^5\text{-}C_5H_5)(P(C_6H_4R)_3)(bipy)][CF_3SO_3]$ (R = F, 3; R = OCH_3, 5). To a stirred and degassed solution of **1** or **2** (0.20 g, 0.25 mmol; 0.13 g, 0.14 mmol, respectively) in dichloromethane (40 mL) were added 2,2′-bipyridine (0.05 g, 0.29 mmol; 0.03 g, 0.17 mmol, for **3** and **5**, respectively) and $AgCF_3SO_3$ (0.09 g, 0.37 mmol; 0.05 g, 0.21 mmol, for **3** and **5**, respectively). After a 6 or 7 h reflux (for **3** or **5**, respectively) the reaction mixture was cooled to room temperature and filtered, and the solvent was removed under vacuum. The dark orange residue was recrystallized from dichloromethane/*n*-hexane, originating **3**, or recrystallized three times from dichloromethane/*n*-hexane, originating **5**, in 87 and 56% yield, respectively. Single crystals were isolated by recrystallization from dichloromethane/*n*-hexane for compounds **3** and **5**.

Complex 3. 87% yield. Dark orange powder. ^1H NMR [$(CD_3)_2CO$, Me_4Si, δ/ppm]: 9.53 (d, 2, $^3J_{HH}$ = 8.0, H_1); 8.25 (d, 2, $^3J_{HH}$ = 8.0, H_4); 7.93 (t, 2, $^3J_{HH}$ = 8.0, H_3); 7.38 (t, 2, $^3J_{HH}$ = 8.0, H_2); 7.14 (m, 12, $P(PhF)_3$); 4.96 (s, 5, $\eta^5\text{-}C_5H_5$). $^{13}C\{^1H\}$ NMR [$(CD_3)_2CO$, δ /ppm]: 164.7 (dd, $^1J_{CF}$ = 250.5; $^4J_{CP}$ = 2.0, Cq, $P(PhF)_3$); 157.4 (d, $^3J_{CP}$ = 2.0, C_1); 156.6 (C_5); 137.3 (C_3); 136.2 (dd, $^3J_{CP}$ = 12.6; $^2J_{CF}$ = 8.0, $CH_{meta}P(PhF)_3$); 128.5 (dd, $^1J_{CP}$ = 43.3; $^4J_{CF}$ = 3.0, Cq, $P(PhF)_3$); 126.3 (C_2); 124.3 (C_4); 116.6 (dd, $^2J_{CP}$ = 21.1; $^3J_{CF}$ = 11.1, $CH_{ortho}P(PhF)_3$); 79.6 (d, $^2J_{CP}$ = 3.0, Cp). $^{31}P\{^1H\}$ NMR [$(CD_3)_2CO$, δ/ppm]: 50.40 (s, $P(PhF)_3$). UV–vis [CH_2Cl_2,

DOI: 10.1021/acs.inorgchem.9b00735
Inorg. Chem. 2019, 58, 9135–9149

λ_{max}/nm ($\varepsilon \times 10^3/M^{-1}cm^{-1}$)]: 290 (25.5); 342 (6.2); 418 (4.6); 473 (Sh). [DMSO, λ_{max}/nm ($\varepsilon \times 10^3/M^{-1}cm^{-1}$)]: 293 (22.2); 352 (Sh); 414 (4.0); 472 (Sh). FTIR [KBr, cm^{-1}]: 3075 (υ_{C-H} Cp and aromatic rings); 1587, 1495 ($\upsilon_{C=C}$ Cp and aromatic rings); 1257 ($\upsilon(CF_3SO_3^-)$). Anal Calcd for $C_{34}H_{25}F_6N_2O_3PRuS$ (787.68): C, 51.9; H, 3.2; N, 3.6; S, 4.1. Found: C, 51.9; H, 3.3; N, 3.5; S, 4.0.

Complex **5**. 56% yield. Dark orange powder. ^1H NMR [$(CD_3)_2CO$, Me_4Si, δ/ppm]: 9.52 (d, 2, $^3J_{HH}$ = 4.0, H_1); 8.18 (d, 2, $^3J_{HH}$ = 8.0, H_4); 7.89 (t, 2, $^3J_{HH}$ = 8.0, H_3); 7.33 (m, 2, H_2); 7.01 (m, 6, $H_{ortho}P(PhOCH_3)_3$), 6.86 (m, 12, $H_{meta}P(PhOCH_3)_3$); 4.89 (s, 5, η^5-C_5H_5); 3.81 (s, 9, OCH_3). $^{13}C\{^1H\}$ NMR [$(CD_3)_2CO$, δ /ppm]: 162.0 (d, $^4J_{CP}$ = 2.0, $CqP(PhOCH_3)_3$); 157.1 (d, $^3J_{CP}$ = 2.0, C_1); 156.6 (C_5); 136.8 (C_3); 135.2 (d, $^2J_{CP}$ = 12.1, $CH_{ortho}P(PhOCH_3)_3$); 125.8 (C_2); 124.2 (C_4); 123.8 (d, $^1J_{CP}$ = 47.3, Cq, $P(PhOCH_3)_3$); 114.7 (d, $^3J_{CP}$ = 10.1, $CH_{meta}P(PhOCH_3)_3$); 79.1 (d, $^2J_{CP}$ = 3.0, Cp); 55.7 (OCH_3). $^{31}P\{^1H\}$ NMR [$(CD_3)_2CO$, δ/ppm]: 47.39 (s, $P(PhOCH_3)_3$). UV−vis [CH_2Cl_2, λ_{max}/nm ($\varepsilon \times 10^3/M^{-1}cm^{-1}$)]: 245 (62.1); 290 (32.5); 352 (Sh); 429 (5.1); 494 (Sh). [DMSO, λ_{max}/nm ($\varepsilon \times 10^3/M^{-1}cm^{-1}$)]: 293 (25.8); 355 (Sh); 425 (4.0); 468 (Sh). FTIR [KBr, cm^{-1}]: 3094−2837 (υ_{C-H} Cp and aromatic rings); 1593−1440 ($\upsilon_{C=C}$ Cp and aromatic rings); 1262 ($\upsilon(CF_3SO_3^-)$). Anal Calcd for $C_{37}H_{34}F_3N_2O_6PRuS$ (823.79): C, 54.0; H, 4.2; N, 3.4; S, 3.9. Found: C, 53.8; H, 4.1; N, 3.1; S, 4.0.

[Ru(η^5-C_5H_5)($P(C_6H_4R)_3$)(bipy−biotin)][CF_3SO_3] (R = F, 4; R = OCH_3, 6). To a stirred and degassed solution of **1** or **2** (0.15 g, 0.18 mmol; 0.33 g, 0.36 mmol, for **4** and **6**, respectively) in methanol (40 mL) were added bipy−biotin (0.15 g, 0.22 mmol; 0.20 g, 0.30 mmol, for **4** and **6**, respectively) and $AgCF_3SO_3$ (0.07 g, 0.27 mmol; 0.12 g, 0.46 mmol, for **4** and **6**, respectively). After a 4 or 7 h reflux (for **4** and **6**, respectively), the reaction mixture was cooled to room temperature and filtered, and the solvent was removed under vacuum. The orange residue was recrystallized twice from methanol/diethyl ether, originating **4**, or three times from dichloromethane/*n*-hexane, originating **6**, in 59 and 52% yield, respectively.

Complex **4**. 59% yield. Orange powder. ^1H NMR [$(CD_3)_2CO$, Me_4Si, δ/ppm]: 9.51 (d, 2, $^3J_{HH}$ = 4.0, H_1); 8.21 (s, 2, H_4); 7.40 (d, 2, $^3J_{HH}$ = 8.0, H_2); 7.15 (m, 12, $P(PhF)_3$); 6.34 (d, 2, $^3J_{HH}$ = 16.0, NH); 6.08 (s, 2, NH); 5.25 (m, 4, H_6); 4.97 (s, 5, η^5-C_5H_5); 4.49 (m, 2, H_{13}); 4.33 (m, 2, H_{12}); 3.21 (m, 2, H_{11}); 2.91 (under the solvent signal, H_{14}); 2.68 (m, 2, H_{14}); 2.50 (m, 4, H_7); 1.72 (m, 4, H_8); 1.62 (m, 4, H_{10}); 1.47 (m, 4, H_9). $^{13}C\{^1H\}$ NMR [$(CD_3)_2CO$, δ /ppm]: 173.5 (C═O ester); 164.7 (dd, $^1J_{CF}$ = 249.5; $^4J_{CP}$ = 2.0, Cq, $P(PhF)_3$); 164.3 (d, C═O biotin); 157.1 (C_1); 156.3 (d, C_5); 147.8 (d, C_3); 136.2 (dd, $^3J_{CP}$ = 13.0; $^2J_{CF}$ = 8.0, $CH_{meta}P(PhF)_3$); 128.3 (dd, $^1J_{CP}$ = 43.3; $^4J_{CF}$ = 4.0, Cq, $P(PhF)_3$); 124.7 (d, C_2); 122.5 (d, C_4); 116.7 (dd, $^2J_{CP}$ = 21.6; $^3J_{CF}$ = 11.1, $CH_{ortho}P(PhF)_3$); 79.6 (d, $^2J_{CP}$ = 2.0, Cp); 64.1 (d, C_6); 62.5 (d, C_{12}); 60.9 (C_{13}); 56.6 (d, C_{11}); 41.1 (d, C_{14}); 34.1 (d, C_7); 29.1 (under the signal of the solvent, C_9, C_{10}); 25.5 (d, C_8). $^{31}P\{^1H\}$ NMR [$(CD_3)_2CO$, δ/ppm]: 50.17 (s, $P(PhF)_3$). UV−vis [CH_2Cl_2, λ_{max}/nm ($\varepsilon \times 10^3/M^{-1}cm^{-1}$)]: 294 (21.1); 338 (Sh); 424 (3.9); 489 (Sh). [DMSO, λ_{max}/nm ($\varepsilon \times 10^3/M^{-1}cm^{-1}$)]: 296 (22.2); 341 (Sh); 420 (4.3); 479 (Sh). FTIR [KBr, cm^{-1}]: 3240 (υ_{NH} amine); 3071 (υ_{C-H} Cp and aromatic rings); 2930, 2860 (υ_{C-H} alkanes); 1732 ($\upsilon_{C=O}$ ester); 1697 ($\upsilon_{C=O}$ ketone); 1495 ($\upsilon_{C=C}$ Cp and aromatic rings); 1260 ($\upsilon(CF_3SO_3^-)$); 1159 (υ_{C-O} ester); 1030 (υ_{C-N} amine). Anal Calcd for $C_{56}H_{57}F_6N_6O_9PRuS_3$ (1300.32): C, 51.7; H, 4.4; N, 6.5; S, 7.4. Found: C, 51.2; H, 4.4; N, 6.2; S, 7.0.

Complex **6**. 52% yield. Orange powder. ^1H NMR [$(CD_3)_2CO$, Me_4Si, δ/ppm]: 9.50 (d, 2, $^3J_{HH}$ = 4.0, H_1), 8.12 (s, 2, H_4), 7.35 (d, 2, $^3J_{HH}$ = 8.0, H_2), 7.01 (m, 6, $H_{ortho}P(PhOCH_3)_3$), 6.86 (m, 6, $H_{meta}P(PhOCH_3)_3$), 6.29 (s, 2, NH), 6.04 (d, 2, $^3J_{HH}$ = 4.0, NH), 5.25 (m, 4, H_6), 4.90 (s, 5, η^5-C_5H_5), 4.49 (m, 2, H_{13}), 4.32 (m, 2, H_{12}), 3.82 (s, 9, OCH_3), 3.22 (m, 2, H_{11}), 2.87 (under the solvent signal, H_{14}), 2.69 (m, 2, H_{14}), 2.50 (m, 4, H_7), 1.71 (m, 4, H_8), 1.63 (m, 4, H_{10}), 1.48 (m, 4, H_9). $^{13}C\{^1H\}$ NMR [$(CD_3)_2CO$, δ /ppm]: 173.6 (d, C═O ester); 164.2 (d, C═O biotin); 162.07 ($^4J_{CP}$ = 2.0, Cq, $P(PhOCH_3)_3$); 157.0 (C_1); 156.4 (d, C_5); 147.2 (d, C_3); 135.4 (d, $^2J_{CP}$ = 13.1, $CH_{ortho}P(PhOCH_3)_3$); 124.3 (d, C_2); 123.7 (d, $^1J_{CP}$ = 46.3, Cq, $P(PhOCH_3)_3$); 122.4 (d, C_4); 114.8 (d, $^3J_{CP}$ = 11.1, $CH_{meta}P(PhOCH_3)_3$); 79.2 (d, $^2J_{CP}$ = 2.0, Cp); 64.2 (d, C_6); 62.6 (d, C_{12}); 60.9 (d, C_{13}); 56.7 (d, C_{11}); 55.8 (OCH_3); 41.2 (d, C_{14}); 34.2 (d, C_7); 29.2 (under the signal of the solvent, C_9, C_{10}); 25.6 (C_8). $^{31}P\{^1H\}$ NMR [$(CD_3)_2CO$, δ/ppm]: 47.13 (s, $P(PhOCH_3)_3$). UV−vis [CH_2Cl_2, λ_{max}/nm ($\varepsilon \times 10^3/M^{-1}cm^{-1}$)]: 246 (51.8); 295 (22.5); 332 (6.6); 437 (3.8); 488 (Sh). [DMSO, λ_{max}/nm ($\varepsilon \times 10^3/M^{-1}cm^{-1}$)]: 296 (22.6); 340 (Sh); 432 (3.7); 480 (Sh). FTIR [KBr, cm^{-1}]: 3360 (υ_{NH} amine); 3073 (υ_{C-H} Cp and aromatic rings); 2932, 2860 (υ_{C-H} alkanes); 1732 ($\upsilon_{C=O}$ ester); 1703 ($\upsilon_{C=O}$ ketone); 1499 ($\upsilon_{C=C}$ Cp and aromatic rings); 1253 ($\upsilon(CF_3SO_3^-)$); 1155 (υ_{C-O} ester); 1030 (υ_{C-N} amine). ESI-MS (+): calcd for $[6]^+$, m/z 1187.31; found, m/z: 1087.21.

X-ray Crystal Structure Determination. Three-dimensional X-ray data were collected on a Bruker Kappa Apex CCD diffractometer at low temperature for the compounds **2**, **3**, **5**, and **LCR134′**, by the $\phi-\omega$ scan method. Reflections were measured from a hemisphere of data collected from frames, each of them covering 0.3° in ω. A total of 63736 for **2**, 45359 for **3**, 48457 for **5**, and 142051 for **LCR134′** reflections measured were corrected for Lorentz and polarization effects and for absorption by multiscan methods based on symmetry-equivalent and repeated reflections. Of the total, 6448 for **2**, 5984 for **3**, 6550 for **5** and 12715 for **LCR134′**, independent reflections exceeded the significance level ($|F|/\sigma|F|$) > 4.0. After data collection, in each case an multiscan absorption correction (SADABS)[54] was applied, and the structure was solved by direct methods and refined by full matrix least-squares on F^2 data using SHELX suite of programs.[55] Olex2 program was used in the refinement of **LCR134′**.[56] Hydrogen atoms were included in calculation position and refined in the riding mode for all structures. Refinements were done with allowance for thermal anisotropy of all non-hydrogen atoms. A final difference Fourier map showed no residual density outside: +0.949 and −0.944 e·Å^{-3} for **2**, +0.538 and −0.583 e·Å^{-3} for **3**, +0.368 and −0.421 e·Å^{-3} for **5** and +1.09 and −0.81 e·Å^{-3} for **LCR134′**. A weighting scheme $w = 1/[\sigma^2(F_o^2) + (0.091800P)^2 + 0.00000P]$ for **2**, $1/[\sigma^2(F_o^2) + (0.033800P)^2 + 0.842800P]$ for **3**, $1/[\sigma^2(F_o^2) + (0.024400P)^2 + 2.362200P]$ for **5**, and $1/[\sigma^2(F_o^2) + (0.142933P)^2 + 0.000000P]$ for **LCR134′**, where $P = (|F_o|^2 + 2|F_c|^2)/3$, were used in the latter stages of refinement. Disordered $CF_3SO_3^-$ and Cl^- anions appear in the crystal packing of **LCR134′**. These disorders have been refined and two atomic sites for the trifluoromethanesulfonic ion and other two atomic sites for the chlorine atom have been observed and refined with the anisotropic atomic displacement parameters. The site occupancy factors were 0.536761 for S(1A)−O(1A)−F(1A)−C(1A)−O(2A)−F(2A)−O(3A)−F(3A) of the $CF_3SO_3^-$ anion and 0.526463 for Cl(2A) of the Cl^- anion. A part of one ring of bipyridine molecule is disordered too. The site occupancy factor was 0.279972 for C(6A)−C(7A). Further details of the crystal structures determination are given in Tables S7−S8. CCDC 1900479−1900482 contain the supplementary crystallographic data for the structures reported in this paper.

Stability Studies in DMSO/DMEM. For the stability studies, all complexes were dissolved in 5% DMSO/95% DMEM at *ca.* 1×10^{-4} M, and their electronic spectra were recorded in the range allowed by the solvents at set time intervals. The samples used in the measurements were protected from light sources and were stored at room temperature between measurements.

Biological Evaluation. *Cell Lines and Culture Conditions.* MCF7 and MDA-MB-231 cells were grown at 37 °C in 5% CO_2 in Dulbecco's modified Eagles's medium (DMEM high glucose) (Capricorn Scientific) supplemented with 10% fetal bovine serum (Capricorn Scientific) and 1% penicillin/streptomycin (Capricorn Scientific). All cells were adherent in monolayers and, upon confluence, were washed with phosphate buffer saline (PBS) 1× and harvested by digestion with trypsin 0.05% (v/v). Trypsin was inactivated by adding fresh complete culture media to the culture flask. Cells were then suspended and transferred into new, sterile, culture flasks or seeded in sterile test plates for the different assays. All cells were manipulated under aseptic conditions in a flow chamber.

DOI: 10.1021/acs.inorgchem.9b00735
Inorg. Chem. 2019, 58, 9135−9149

Compounds Dilution and Storage. All compounds were dissolved in 100% DMSO and divided in aliquots of 10 μL each. Afterward, they were stored at −20 °C until use.

Compound Cytotoxicity Evaluated by MTT Assay. The cells were adherent in monolayers and, upon confluency, were harvested by digestion with trypsin−EDTA. The cytotoxicity of the complexes against the tumor cells was assessed using the colorimetric assay MTT (3-(4,5-2-yl)-2,5-ditetrazolium bromide), which measures the conversion of the yellow tetrazolium into purple formazan by mitochondrial redox activity in living cells. For this purpose, cells ((10−20) × 10^3 in 200 μL of medium) were seeded into 96-well plates and incubated in a 5% CO_2 incubator at 37 °C. Cells settled for 24 h followed by the addition of a dilution series of the complexes in medium (200 μL). The complexes and ligands were first solubilized in 100% DMSO, given a 10 mM stock solution, then in medium within the concentration range 0.01−100 μM for the complexes and 10−200 μM for phosphane- and bipyridine-based ligands. DMSO did not exceed 1% even for the higher concentration used, and it was without cytotoxic effect. After 24 h of incubation, the treatment solutions were removed by aspiration, and MTT solution (200 μL, 0.5 mg/mL in PBS) was added to each well. After 3−4 h at 37 °C/5% CO_2, the solution was removed, and the purple formazan crystals formed inside the cells were dissolved in DMSO (200 μL) by thorough shaking. The cellular viability was evaluated by measuring the absorbance at 570 nm by using a microplate spectrophotometer.

Compound Cytotoxicity Evaluated by SRB Assay. MDA-MB-231 cells were seeded at a concentration of 4 × 10^4 cells/mL, in 24-well test plates. After 24 h of seeding, cells were incubated with different concentrations of the **LCR134**, **4**, and **6** compounds for 48 h. For each cell line and compound, two negative controls were performed, a control (1) in which cells were incubated only with growth medium and a DMSO control (2) in which the cells were exposed to the highest concentration used of DMSO (maximum of 0.1% DMSO per well (v/v)), to discard any influence of this solvent in the results. After a 48 h treatment, cells were fixed in ice-cold methanol containing 1% acetic acid for at least 90 min at −20 °C. Fixing solution was then removed, and the plate was left air-dry at room temperature; then, the fixed cells were incubated with 0.5% (w/v) SRB dissolved in 1% acetic acid for 90 min at 37 °C protected from light. After washing with 1% acetic acid and air-drying at room temperature, SRB was solubilized with 10 mM Tris pH 10. Absorbance was read at 540 nm in a microplate spectrophotometer (Bio Tek Synergy HT). Results were expressed relatively to the negative control (1), which was considered as 100% of cell growth.

Biotin−Avidin Interaction Assay. The biotin−avidin interactions of the compounds **3** and **5**, bearing 2,2′-bipyridine ligand and the biotinylated complexes **4**, **6**, and **LCR134** were measured by using a Pierce Biotin Quantitation kit (ThermoScientific) according to the manufacturer's protocol. For this purpose, 100 μL of MQ water was added to each tube of HABA/Avidin premix, after it was equilibrated at room temperature. Then, 160 μL of PBS was added to each microplate well, followed by addition of 20 μL of HABA/Avidin premix solution. The microplate was placed in a microplate spectrophotometer, mixed and the absorbance measured at 500 nm. After recording the absorbance values, 20 μL of complexes **3**−**6** and LCR134 or biotin (positive control), at a concentration of 10 μM, were added to the well containing the HABA/Avidin mixture and mixed. The absorbance values were measured again at 500 nm from time to time, until values remained constant. A solution containing 0.1% DMSO or water were used as negative controls.

Cellular Uptake Measured by ICPMS Analysis. For the cellular uptake experiments, MDA-MB-231 and MCF7 cells (ca. 1 × 10^6 and 2 × 10^6 cells, respectively in 5 mL medium) were seeded into t25 flasks and incubated in a 5% CO_2 incubator at 37 °C. Cells settled for 24 h, followed by the addition of **LCR134**, **4**, and **6** at a concentration equivalent to their IC_{50} values found for 24 h challenge at 37 °C. After incubation, cells were washed with ice-cold PBS and treated in order to obtain a cellular pellet. The cytosol, membrane/particulate, cytoskeletal, and nuclear fractions were extracted using a Fraction-PREP (BioVision, USA) cell fractionation kit according to the manufacturer's protocol. The Ru (^{101}Ru) content in each fraction was measured by a Thermo X-Series Quadrupole ICPMS (Thermo Scientific) after digestion of the samples and using the same procedure previously described.[47]

Cell Death Measurement by Flow Cytometry−Annexin V/PI Assay. After a 48 h treatment with compounds **LCR134**, **4**, and **6**, both suspended and attached cells were collected and washed in 1× PBS. Then 1 × 10^6 cells were resuspended in 100 μL of 1× binding buffer and incubated with 5 μL AV- fluorescein isothiocyanate (BD Biosciences, San Jose, CA) and 5 μL of PI (50 μg/mL) for 15 min in the dark. Samples were analyzed using CytoFLEX Cytometer (Beckman Coulter) in an Epics XLTM (Beckman Coulter) cytometer, equipped with an argon-ion laser emitting a 488 nm beam at 15 mW. Monoparametric detection of red fluorescence was performed using FL-4 (488/675 nm) and detection of green fluorescence was performed using FL-1 (488/525 nm). Then 20 000 cells were analyzed per sample, and data were analyzed using FlowJo software (version 7.6, Tree Star Inc., Ashland, OR).

Colony Formation Assay. MDA-MB-231 were seeded in 6-well plates at 300 cells/mL. Then, 24 h after plating, cells were incubated with $^1/_4$ IC_{50} and IC_{50} values of compounds **LCR134**, **4**, and **6**. 48 h after the incubation, old medium was removed, and cells were incubated with fresh medium. Medium was renewed every 3 days. Eleven days after removing the treatments, cells were washed with PBS and incubated in a solution of glutaraldehyde (6% (v/v)) with crystal violet (0.5% (w/v)) for at least half an hour. The plate was washed with fresh water and left air-dry. Colonies were counted manually. The negative control was incubated with the correspondent volume of DMSO used in the solubilization of the compounds (vehicle), and the final concentration of DMSO per well did not exceed 0.1%.

In Vivo Toxicity Assessment Using Zebrafish Embryos. The AB strain zebrafish (Zebrafish International Resource Center, Eugene, OR) was used for all experiments. Breeding stocks were bred and housed in Aquatic Habitats (Apopka, FL) recirculating systems under a 14/10 h light/dark cycle. System water was obtained by carbon/sand filtration of municipal tap water and water quality was maintained at <0.05 ppm nitrite, < 0.2 ppm ammonia, pH between 7.2 and 7.7, and water temperature between 26 and 28 °C. All experiments were conducted in accordance with the zebrafish husbandry protocol and embryonic exposure protocol (#08−025) approved by the Rutgers University Animal Care and Facilities Committee.

Males and females were maintained separately and comingled the night before to allow spawning the next morning. Spawning substrates were placed into the fish tanks on the day prior to spawning. In case eggs were obtained from more than one set of breeders, all eggs that were fertilized and progressing normally through development were mixed.

Zebrafish embryos were exposed to different concentrations of compounds **3**, **4**, **5**, and **6** (Table 3), at 0.05% of DMSO in individual glass vials through a waterborne exposure from 3 h postfertilization (hpf) until 120 hpf (5 days) in a static nonrenewal protocol. The solutions were prepared from compound **3**, **4**, **5**, and **6** stock solution of 7.79, 115.80, 5.30, and 92.56 mg/L, respectively.

The exposure followed a modified OECD 236 protocol,[50] where the end points of lesion presence, length, and mortality were recorded, during the major stages of organ development and the toxicological estimates (LC_{50}, NOEC, LOEC and NOAEL) were determined. Those embryos surviving at the end of the toxicological experiment (120 hpf) were used for both morphological data and ICPMS Ru quantification analysis. For morphological data, approximately 12 individual larvae from each complex concentration and control group were fixed in formalin and then stained for bone and cartilage following a two-color acid free Alcian blue/Alizarin red stain.[57] Photographs were taken using a Scion digital camera model CFW-1310C mounted on an Olympus SZ-PT dissecting microscope, and cartilage/bone were measured using Adobe Photoshop. End points examined included total body length, intraocular distance, and yolk sac and pericardial sac size to assess larval growth, cranial facial

DOI: 10.1021/acs.inorgchem.9b00735
Inorg. Chem. 2019, 58, 9135−9149

Table 3. Analytically Evaluated Concentrations by ICPMS at the End of the Experiment (120 hpf Experiment)[a]

complex	solutions (mg/L)	std	larvae (ng/embryo)	std
3	ND (control)	–	ND (control)	–
	0.69	0.16	1.56	0.40
	2.02	0.26	3.37	0.74
	3.18	0.41	4.93	0.70
	3.57	0.26	–	–
4	ND (control)	–	ND (control)	–
	1.31	0.08	1.89	0.79
	1.79	0.08	1.93	0.23
	2.03	0.21	3.79	1.03
	2.44	0.42	–	–
	2.56	0.29	–	–
	8.77	0.58	–	–
	19.19	0.23	–	–
5	ND (control)	–	ND (control)	–
	0.02	0.01	0.23	0.08
	0.04	0.01	0.49	0.08
	0.17	0.03	0.92	0.12
	0.57	0.05	3.57	1.57
	0.92	0.20	–	–
	1.20	0.27	–	–
	1.36	0.11	–	–
6	ND (control)	–	ND (control)	–
	0.63	0.12	0.86	0.12
	0.80	0.13	1.17	0.10
	1.52	0.40	–	–
	3.01	0.54	–	–

[a]The ruthenium (element) concentrations given by ICPMS in μg/L (ppb) were converted to concentrations of each complex, in mg/L or ng/embryo. ND: Not detected.

development, and nutrient storage and usage, respectively (Figures S4–S7). For the analytical data, the solutions in each vial were collected for ICPMS analysis, and the larvae were euthanized and fixed with 10% buffered formalin phosphate.[58] Three replicates containing larvae from each concentration were also collected for ICPMS analysis (see below).

The concentrations of each individual compounds and corresponding control groups were set up as individual experiments, and the sample size was between 30 and 40 embryos, and repeated two times. The controls had ≥90% survival rate.

Quantification of Ruthenium Element by Inductively Coupled Plasma Mass Spectrometry (ICPMS). Samples were quantified via high resolution ICPMS (Nu Instruments Attom, U.K.) at Rutgers EOHSI Analytical Facility. The instrument settings for the ICPMS are provided in Table 4. Larval samples were microwave digested using a MARS X microwave digester (CEM Matthews NC) in OmniTrace Nitric acid and diluted to 3.5% acid with 30% hydrogen peroxide solution (Sigma-Aldrich). Spiked egg water treatments were acidified to 3.5%. The samples were introduced through a ASX-500 Model 510 Auto Sampler (Cetac) and into a Gass Expansion Conikal Nebulizer within the Peltier cooling system. Data was sent into the Attom software (Attolab v.1) and analyzed with NuQuant by using a seven-point calibration curve. The limit of quantification for these samples was 0.005 ppb and ruthenium isotopes 99, 100, 101, and 102 were quantified. It is important to note that an oxide of strontium, an ingredient in salt water solutions, like egg water, has considerable isobaric interference for ruthenium 100. No isobaric interferences were noted for larval samples. The ruthenium concentrations given by ICPMS in μg/L (ppb) were converted to concentrations in mg/L, for each complex.

Table 4. ICPMS Method Parameters

method settings	parameter
analysis mode	deflector jump, single mass jump
dwell time per peak	4 ms
switch delay per peak (×10 μs)	2
number of sweeps	450
number of cycles	1
instrument resolutuion	300
scan window (%)	0
peak center mass	none
detection mode	attenuated
park mass	98.90594

■ ASSOCIATED CONTENT

Supporting Information

The Supporting Information is available free of charge on the ACS Publications website at DOI: 10.1021/acs.inorgchem.9b00735.

X-ray data (bond lengths and angles, crystal data, and structure refinement; enantiomers present in the crystal packing), stability curves, summary of the most observed toxic lesions in the zebrafish larvae exposed to different doses of complexes, lethality-response curve for tested compounds in zebrafish, morphometric measurements in zebrafish, and cell viability assays (PDF)

Accession Codes

CCDC 1900479–1900482 contain the supplementary crystallographic data for this paper. These data can be obtained free of charge via www.ccdc.cam.ac.uk/data_request/cif, or by emailing data_request@ccdc.cam.ac.uk, or by contacting The Cambridge Crystallographic Data Centre, 12 Union Road, Cambridge CB2 1EZ, UK; fax: +44 1223 336033.

■ AUTHOR INFORMATION

Corresponding Authors

*(A.V.) E-mail: amvalente@fc.ul.pt.
*(M.H.G.) E-mail: mhgarcia@fc.ul.pt.

ORCID

Andreia Valente: 0000-0002-3370-208X

Notes

The authors declare no competing financial interest.

■ ACKNOWLEDGMENTS

This work was financed by the Portuguese Foundation for Science and Technology (Fundação para a Ciência e Tecnologia, FCT) within the scope of Projects UID/QUI/00100/2019 and PTDC/QUI-QIN/28662/2017. This work was supported by the strategic program UID/BIA/04050/2013 (POCI-01-0145-FEDER-007569) funded by national funds through the FCT I.P. and by the ERDF through the COMPETE2020 - Programa Operacional Competitividade e Internacionalização (POCI). A.V. acknowledges the Investigator FCT2013 Initiative for the Project IF/01302/2013 and CEEC-IND/01974/2017 (acknowledging FCT, as well as POPH and FSE, the European Social Fund). L.C.-R., A.R.B. and A.P. thank FCT for their Ph.D. Grants (SFRH/BD/100515/2014, SFRH/BD/139271/2018, and SFRH/BD/139412/2018, respectively). L.C.-R. also acknowledges Fulbright Research Grant 2017/2018 with the support of FCT. Brittany Karas acknowledges NJAES-RutgersNJ01201 and NIEHS Training Grant T32-ES 007148 and B.T.B. and C.D.

DOI: 10.1021/acs.inorgchem.9b00735
Inorg. Chem. 2019, 58, 9135–9149

acknowledge NIH-NIEHS P30 ES005022. K.R.C. acknowledges NJAES Project 01202 (W2045) and NIH ES005022.

REFERENCES

(1) Bareford, L. M.; Avaritt, B. R.; Ghandehari, H.; Nan, A.; Swaan, P. W. Riboflavin-Targeted Polymer Conjugates for Breast Tumor Delivery. *Pharm. Res.* **2013**, *30* (7), 1799−1812.
(2) Waibel, R.; Treichler, H.; Schaefer, N. G.; Van Staveren, D. R.; Mundwiler, S.; Kunze, S.; Küenzi, M.; Alberto, R.; Nüesch, J.; Knuth, A.; et al. New Derivatives of Vitamin B12 Show Preferential Targeting of Tumors. *Cancer Res.* **2008**, *68* (8), 2904−2911.
(3) Paulos, C. M.; Turk, M. J.; Breur, G. J.; Low, P. S. Folate Receptor-Mediated Targeting of Therapeutic and Imaging Agents to Activated Macrophages in Rheumatoid Arthritis. *Adv. Drug Delivery Rev.* **2004**, *56* (8), 1205−1217.
(4) Russell-Jones, G.; McTavish, K.; McEwan, J.; Rice, J.; Nowotnik, D. Vitamin-Mediated Targeting as a Potential Mechanism to Increase Drug Uptake by Tumours. *J. Inorg. Biochem.* **2004**, *98* (10), 1625−1633.
(5) Ren, W. X.; Han, J.; Uhm, S.; Jang, Y. J.; Kang, C.; Kim, J. H.; Kim, J. S. Recent Development of Biotin Conjugation in Biological Imaging, Sensing, and Target Delivery. *Chem. Commun.* **2015**, *51* (52), 10403−10418.
(6) Collina, S.; Tripodo, G.; Mandracchia, D.; Rui, M.; Rossi, D. New Perspectives in Cancer Therapy: The Biotin-Antitumor Molecule Conjugates. *Med. Chem. (Los. Angeles)* **2014**, *S1* (4), 1−8.
(7) Chen, S.; Zhao, X.; Chen, J.; Chen, J.; Kuznetsova, L.; Wong, S. S.; Ojima, I. Mechanism-Based Tumor-Targeting Drug Delivery System. Validation of Efficient Vitamin Receptor-Mediated Endocytosis and Drug Release. *Bioconjugate Chem.* **2010**, *21* (5), 979−987.
(8) Lis, L. G.; Smart, M. A.; Luchniak, A.; Gupta, M. L.; Gurvich, V. J. Synthesis and Biological Evaluation of a Biotinylated Paclitaxel with an Extra-Long Chain Spacer Arm. *ACS Med. Chem. Lett.* **2012**, *3* (9), 745−748.
(9) Singh, Y.; Durga Rao Viswanadham, K. K.; Kumar Jajoriya, A.; Meher, J. G.; Raval, K.; Jaiswal, S.; Dewangan, J.; Bora, H. K.; Rath, S. K.; Lal, J.; et al. Click Biotinylation of PLGA Template for Biotin Receptor Oriented Delivery of Doxorubicin Hydrochloride in 4T1 Cell-Induced Breast Cancer. *Mol. Pharmaceutics* **2017**, *14* (8), 2749−2765.
(10) Maiti, S.; Park, N.; Han, J. H.; Jeon, H. M.; Lee, J. H.; Bhuniya, S.; Kang, C.; Kim, J. S. Gemcitabine-Coumarin-Biotin Conjugates: A Target Specific Theranostic Anticancer Prodrug. *J. Am. Chem. Soc.* **2013**, *135* (11), 4567−4572.
(11) Hu, W.; Fang, L.; Hua, W.; Gou, S. Biotin-Pt (IV)-Indomethacin Hybrid: A Targeting Anticancer Prodrug Providing Enhanced Cancer Cellular Uptake and Reversing Cisplatin Resistance. *J. Inorg. Biochem.* **2017**, *175* (June), 47−57.
(12) Trondl, R.; Heffeter, P.; Kowol, C. R.; Jakupec, M. A.; Berger, W.; Keppler, B. K. NKP-1339, the First Ruthenium-Based Anticancer Drug on the Edge to Clinical Application. *Chem. Sci.* **2014**, *5* (8), 2925−2932.
(13) Alessio, E.; Messori, L. The Deceptively Similar ruthenium(III) Drug Candidates KP1019 and NAMI-A Have Different Actions. What Did We Learn in the Past 30 Years? *Met. Ions Life Sci.* **2018**, *18*, 141−170.
(14) Jakupec, M. A.; Kandioller, W.; Schoenhacker-Alte, B.; Trondl, R.; Berger, W.; Keppler, B. K. Trends and Perspectives of Ruthenium Anticancer Compounds (Non-PDT). *Ruthenium Complexes: Photochemical and Biomedical Applications* **2017**, 271−291.
(15) Murray, B. S.; Babak, M. V.; Hartinger, C. G.; Dyson, P. J. The Development of RAPTA Compounds for the Treatment of Tumors. *Coord. Chem. Rev.* **2016**, *306* (P1), 86−114.
(16) Dougan, S. J.; Sadler, P. J. The Design of Organometallic Ruthenium Arene Anticancer Agents. *Chimia* **2007**, *61* (11), 704−715.
(17) Morais, T. S.; Valente, A.; Tomaz, A. I.; Marques, F.; Garcia, M. H. Tracking Antitumor Metallodrugs: Promising Agents with the Ru(II)- and Fe(II)-Cyclopentadienyl Scaffolds. *Future Med. Chem.* **2016**, *8* (5), 527−544.
(18) Scalambra, F.; Lorenzo-Luis, P.; de los Ríos, I.; Romerosa, A. New Findings in Metal Complexes with Antiproliferative Activity Containing 1,3,5-Triaza-7-Phosphaadamantane (PTA) and Derivative Ligands. *Eur. J. Inorg. Chem.* **2019**, *2019*, 1529−1538.
(19) Gano, L.; Pinheiro, T.; Matos, A. P.; Tortosa, F.; Jorge, T. F.; Gonçalves, M. S.; Martins, M.; Morais, T. S.; Tomaz, A. I.; Valente, A.; et al. Antitumour and Toxicity Evaluation of a Ru(II)-Cyclopentadienyl Complex in a Prostate Cancer Model by Imaging Tools. *Anticancer. Agents Med. Chem.* **2019**, DOI: 10.2174/1871520619666190318152726.
(20) Mendes, N.; Tortosa, F.; Valente, A.; Marques, F.; Matos, A.; Morais, T. S.; Tomaz, A. I.; Gärtner, F.; Garcia, M. H. In Vivo Performance of a Ruthenium-Cyclopentadienyl Compound in an Orthotopic Triple Negative Breast Cancer Model. *Anticancer. Agents Med. Chem.* **2017**, *17*, 126−136.
(21) Babak, M. V.; Plazuk, D.; Meier, S. M.; Arabshahi, H. J.; Reynisson, J.; Rychlik, B.; Błauz, A.; Szulc, K.; Hanif, M.; Strobl, S.; et al. Half-Sandwich Ruthenium(II) Biotin Conjugates as Biological Vectors to Cancer Cells. *Chem. - Eur. J.* **2015**, *21* (13), 5110−5117.
(22) Siewert, B.; Langerman, M.; Pannwitz, A.; Bonnet, S. Synthesis and Avidin Binding of Ruthenium Complexes Functionalized with a Light-Cleavable Free Biotin Moiety. *Eur. J. Inorg. Chem.* **2018**, *2018* (37), 4107.
(23) Côrte-Real, L.; Paula Robalo, M.; Marques, F.; Nogueira, G.; Avecilla, F.; Silva, T. J. L.; Santos, F. C.; Isabel Tomaz, A.; Helena Garcia, M.; Valente, A. The Key Role of Coligands in Novel ruthenium(II)-Cyclopentadienyl Bipyridine Derivatives: Ranging from Non-Cytotoxic to Highly Cytotoxic Compounds. *J. Inorg. Biochem.* **2015**, *150*, 148−159.
(24) Côrte-Real, L.; Mendes, F.; Coimbra, J.; Morais, T. S.; Tomaz, A. I.; Valente, A.; Garcia, M. H.; Santos, I.; Bicho, M.; Marques, F. Anticancer Activity of Structurally Related ruthenium(II) Cyclopentadienyl Complexes. *J. Biol. Inorg. Chem.* **2014**, *19* (6), 853−867.
(25) Valente, A.; Garcia, M. H.; Marques, F.; Miao, Y.; Rousseau, C.; Zinck, P. First Polymer "ruthenium-Cyclopentadienyl" complex as Potential Anticancer Agent. *J. Inorg. Biochem.* **2013**, *127*, 79−81.
(26) Morais, T. S.; Valente, A.; Tomaz, A. I.; Marques, F.; Garcia, M. H. Tracking Antitumor Metallodrugs: Promising Agents with the Ru(II)- and Fe(II)-Cyclopentadienyl Scaffolds. *Future Med. Chem.* **2016**, *8* (5), 527−544.
(27) Moreira, T.; Francisco, R.; Comsa, E.; Duban-Deweer, S.; Labas, V.; Teixeira-Gomes, A. P.; Combes-Soia, L.; Marques, F.; Matos, A.; Favrelle, A.; et al. Polymer "ruthenium-Cyclopentadienyl" Conjugates - New Emerging Anti-Cancer Drugs. *Eur. J. Med. Chem.* **2019**, *168*, 373−384.
(28) Côrte-Real, L.; Karas, B.; Gírio, P.; Moreno, A.; Avecilla, F.; Marques, F.; Buckley, B. T.; Cooper, K. R.; Doherty, C.; Falson, P.; et al. Unprecedented Inhibition of P-Gp Activity by a Novel Ruthenium-Cyclopentadienyl Compound Bearing a Bipyridine-Biotin Ligand. *Eur. J. Med. Chem.* **2019**, *163*, 853−863.
(29) Florindo, P. R.; Pereira, D. M.; Borralho, P. M.; Rodrigues, C. M. P.; Piedade, M. F. M.; Fernandes, A. C. Cyclopentadienyl-ruthenium(II) and iron(II) Organometallic Compounds with Carbohydrate Derivative Ligands as Good Colorectal Anticancer Agents. *J. Med. Chem.* **2015**, *58* (10), 4339−4347.
(30) Bruce, M. I.; Windsor, N. J. Cyclopentadienyl-Ruthenium and -Osmium Chemistry. IV. Convenient High-Yield Synthesis of Some Cyclopentadienyl Ruthenium or Osmium Tertiary Phosphine Halide Complexes. *Aust. J. Chem.* **1977**, *30* (7), 1601−1604.
(31) Côrte-Real, L.; Teixeira, R. G.; Gírio, P.; Comsa, E.; Moreno, A.; Nasr, R.; Baubichon-Cortay, H.; Avecilla, F.; Marques, F.; Robalo, M. P.; et al. Methyl-Cyclopentadienyl Ruthenium Compounds with 2,2′-Bipyridine Derivatives Display Strong Anticancer Activity and Multidrug Resistance Potential. *Inorg. Chem.* **2018**, *57*, 4629−4639.
(32) Teixeira, R. G.; Brás, A. R.; Côrte-Real, L.; Tatikonda, R.; Sanches, A.; Robalo, M. P.; Avecilla, F.; Moreira, T.; Garcia, M. H.; Haukka, M.; et al. Novel Ruthenium Methylcyclopentadienyl

DOI: 10.1021/acs.inorgchem.9b00735
Inorg. Chem. 2019, 58, 9135−9149

Complex Bearing a Bipyridine Perfluorinated Ligand Shows Strong Activity towards Colorectal Cancer Cells. *Eur. J. Med. Chem.* **2018**, *143*, 503−514.
(33) Moreno, V.; Font-Bardia, M.; Calvet, T.; Lorenzo, J.; Avilés, F. X.; Garcia, M. H.; Morais, T. S.; Valente, A.; Robalo, M. P. DNA Interaction and Cytotoxicity Studies of New ruthenium(II) Cyclopentadienyl Derivative Complexes Containing Heteroaromatic Ligands. *J. Inorg. Biochem.* **2011**, *105* (2), 241−249.
(34) Govindaswamy, P.; Linder, D.; Lacour, J.; Süss-Fink, G.; Therrien, B. Chiral or Not Chiral? A Case Study of the Hexanuclear Metalloprisms [Cp(6)M(6)(micro(3)-Tpt-kappaN)(2)(micro-C2O4-kappaO)(3)]6+ (M = Rh, Ir, Tpt = 2,4,6-Tri(pyridin-4-Yl)-1,3,5-Triazine. *Dalton Trans.* **2007**, *6*, 4457−4463.
(35) Feng, Y.; Deng, Q.; Peng, C.; Hu, J.; Li, Y.; Wu, Q.; Xu, Z. Ultrahigh Discharged Energy Density Achieved in Inhomogeneous PVDF Dielectric Composite Filled with 2D MXene Nanosheets via Interface Engineering. *J. Mater. Chem. C* **2018**, *5*, 876−881.
(36) Nikolić, S.; Opsenica, D. M.; Filipović, V.; Dojčinović, B.; Arandelović, S.; Radulović, S.; Grgurić-Šipka, S. Strong in Vitro Cytotoxic Potential of New Ruthenium-Cymene Complexes. *Organometallics* **2015**, *34* (14), 3464−3473.
(37) Pantić, D. N.; Arandelović, S.; Radulović, S.; Roller, A.; Arion, V. B.; Grgurić-Šipka, S. Synthesis, Characterisation and Cytotoxic Activity of organoruthenium(II)-Halido Complexes with 1H-Benzimidazole-2-Carboxylic Acid. *J. Organomet. Chem.* **2016**, *819*, 61−68.
(38) Nikolić, S.; Rangasamy, L.; Gligorijević, N.; Arandelović, S.; Radulović, S.; Gasser, G.; Grgurić-Šipka, S. Synthesis, Characterization and Biological Evaluation of Novel Ru(II)-Arene Complexes Containing Intercalating Ligands. *J. Inorg. Biochem.* **2016**, *160*, 156−165.
(39) Colina-Vegas, L.; Luna-Dulcey, L.; Plutín, A. M.; Castellano, E. E.; Cominetti, M. R.; Batista, A. A. Half Sandwich Ru(II)-Acylthiourea Complexes: DNA/HSA-Binding, Anti-Migration and Cell Death in a Human Breast Tumor Cell Line. *Dalt. Trans.* **2017**, *46* (38), 12865−12875.
(40) Biancalana, L.; Zacchini, S.; Ferri, N.; Lupo, M. G.; Pampaloni, G.; Marchetti, F. Tuning the Cytotoxicity of Ruthenium(ii) Para-Cymene Complexes by Mono-Substitution at a Triphenylphosphine/phenoxydiphenylphosphine Ligand. *Dalt. Trans.* **2017**, *46* (47), 16589−16604.
(41) Gopalakrishnan, D.; Ganeshpandian, M.; Loganathan, R.; Bhuvanesh, N. S. P.; Sabina, X. J.; Karthikeyan, J. Water Soluble Ru(II)-Arene Complexes of the Antidiabetic Drug Metformin: DNA and Protein Binding, Molecular Docking, Cytotoxicity and Apoptosis-Inducing Activity. *RSC Adv.* **2017**, *7* (60), 37706−37719.
(42) Mohamed Kasim, M. S.; Sundar, S.; Rengan, R. Synthesis and Structure of New Binuclear ruthenium(II) Arene Benzil Bis-(benzoylhydrazone) Complexes: Investigation on Antiproliferative Activity and Apoptosis Induction. *Inorg. Chem. Front.* **2018**, *5*, 585−596.
(43) Ramadevi, P.; Singh, R.; Jana, S. S.; Devkar, R.; Chakraborty, D. Mixed Ligand Ruthenium Arene Complexes Containing N-Ferrocenyl Amino Acids: Biomolecular Interactions and Cytotoxicity against MCF7 Cell Line. *J. Organomet. Chem.* **2017**, *833*, 80−87.
(44) Mondal, A.; Tripathy, R. K.; Dutta, P.; Santra, M. K.; Isab, A. A.; Bielawski, C. W.; Kisan, H. K.; Chandra, S. K.; Dinda, J. Ru(II)-Based Antineoplastic: A "wingtip" N-Heterocyclic Carbene Facilitates Access to a New Class of Organometallics That Are Cytotoxic to Common Cancer Cell Lines. *Appl. Organomet. Chem.* **2019**, *33* (1), e4692.
(45) Lee, R. F. S.; Escrig, S.; Maclachlan, C.; Knott, G. W.; Meibom, A.; Sava, G.; Dyson, P. J. The Differential Distribution of RAPTA-T in Non-Invasive and Invasive Breast Cancer Cells Correlates with Its Anti-Invasive and Anti-Metastatic Effects. *Int. J. Mol. Sci.* **2017**, *18* (9), 1869.
(46) Matos, A.; Mendes, F.; Valente, A.; Morais, T.; Tomaz, A. I.; Zinck, P.; Garcia, M. H.; Bicho, M. B.; Marques, F. Ruthenium-Based Anticancer Compounds: Insights into Their Cellular Targeting and Mechanism of Action. *Ruthenium Complexes: Photochemical and Biomedical Applications* **2017**, 201−219.
(47) Côrte-Real, L.; Matos, A. P.; Alho, I.; Morais, T. S.; Tomaz, A. I.; Garcia, M. H.; Santos, I.; Bicho, M. P.; Marques, F. Cellular Uptake Mechanisms of an Antitumor Ruthenium Compound: The Endosomal/lysosomal System as a Target for Anticancer Metal-Based Drugs. *Microsc. Microanal.* **2013**, *19* (5), 1122−1130.
(48) Gutiérrez-Lovera, C.; Vázquez-Ríos, A. J.; Guerra-Varela, J.; Sánchez, L.; de la Fuente, M. The Potential of Zebrafish as a Model Organism for Improving the Translation of Genetic Anticancer Nanomedicines. *Genes (Basel)* **2017**, *8* (12), 349.
(49) Garcia, G. R.; Noyes, P. D.; Tanguay, R. L. Advancements in Zebrafish Applications for 21st Century Toxicology. *Pharmacol. Ther.* **2016**, *161*, 11−21.
(50) OECD. Test No. 236: Fish Embryo Acute Toxicity (FET) Test. *OECD Guidelines for the Testing of Chemicals, Section 2* **2013**, 1−22.
(51) Côrte-Real, L.; Mendes, F.; Coimbra, J.; Morais, T. S.; Tomaz, A. I.; Valente, A.; Garcia, M. H.; Santos, I.; Bicho, M.; Marques, F. Anticancer Activity of Structurally Related ruthenium(II) Cyclopentadienyl Complexes. *JBIC, J. Biol. Inorg. Chem.* **2014**, *19* (6), 853−867.
(52) Abramson, V. G.; Lehmann, B. D.; Ballinger, T. J.; Pietenpol, J. A. Subtyping of Triple-Negative Breast Cancer: Implications for Therapy. *Cancer* **2015**, *121* (1), 8−16.
(53) Dasari, S.; Tchounwou, P. B. Cisplatin in Cancer Therapy: Molecular Mechanisms of Action. *Eur. J. Pharmacol.* **2014**, *740*, 364−378.
(54) Sheldrick, G. M. *SADABS*, Version 2.10; University of Göttingen: Göttingen, Germany, 2004.
(55) Sheldrick, G. M. Crystal Structure Refinement with SHELXL. *Acta Crystallogr., Sect. C: Struct. Chem.* **2015**, *71* (Md), 3−8.
(56) Dolomanov, O. V.; Bourhis, L. J.; Gildea, R. J.; Howard, J. A. K.; Puschmann, H. OLEX2: A Complete Structure Solution, Refinement and Analysis Program. *J. Appl. Crystallogr.* **2009**, *42* (2), 339−341.
(57) Walker, M. B.; Kimmel, C. B. A Two-Color Acid-Free Cartilage and Bone Stain for Zebrafish Larvae. *Biotech. Histochem.* **2007**, *82* (1), 23−28.
(58) Karas, B. F.; Côrte-Real, L.; Doherty, C. L.; Valente, A.; Cooper, K. R.; Buckley, B. T. A Novel Screening Method for Transition Metal-Based Anticancer Compounds Using Zebrafish Embryo-Larval Assay and Inductively Coupled Plasma-Mass Spectrometry Analysis. *J. Appl. Toxicol.* **2019**, 1−8.

DOI: 10.1021/acs.inorgchem.9b00735
Inorg. Chem. 2019, 58, 9135−9149